Diplomarbeit

Quality Control of ATLAS Muon Chambers

ausgeführt am

Institut für Kernphysik (E142)

der Technischen Universität Wien

unter der Anleitung von Ao. Univ. Prof. Dr. Christian W. Fabjan

durch

Adrian Fabich

im Rahmen der

ATLAS Muon Collaboration, CERN

CH-1211 Genf 23

CERN-THESIS-99-078
//1999

Dezember 1999

Kurzfassung

ATLAS ist ein Universalexperiment für den geplanten Large Hadron Collider (LHC) am CERN. Das Myonspektrometer von ATLAS wird aus Präzisionskammern mit einer Gesamtfläche von $\sim$ 5500 m^2 bestehen und Myonentrajektorien entlang eines 5 m bis 15 m langen Spektrometerarms in einem Magnetfeld von $\sim$ 0.5 T messen. Als Präzisionsdetektoren im Myonspektrometer werden 370.000 Hochdruckdriftrohre (MDTs), zusammengesetzt zu etwa 1200 Präzisionsdrahtkammern, verwendet werden.

Das Signalverhalten der MDT Röhren hängt in starkem Masse von der Qualität der Montage ab. Ein einheitliches und stabiles Verhalten kann nur durch intensive Qualitätskontrolle während der Produktion gewährleistet werden. Gasdichtheit, Hochspannungsverhalten und Dunkelstrom sind globale Parameter, die für alle Gasdetektoren gültig sind. Jede MDT Kammer wird nach der Fertigung unmittelbar bei der Produktionsstätte geprüft. Funktionsprüfungen, z.B. mit radioaktiven Quellen und kosmischer Strahlung, werden durchgeführt, um ausführliche Leistungsdaten zu erhalten.

Ein Hauptmerkmal der MDT Röhren, die Gasdichtheit, und deren Überprüfung sind das Thema dieser Diplomarbeit. Der Gasdruck innerhalb der Röhren ist 3 bar, gefüllt mit Ar/CO_2 93/7. Die geforderte Auflösung macht es notwendig, eine maximal erlaubte Leckrate von $2 * 10^{-8} \frac{bar\ l}{s}$ für MDT Kammern zu definieren. Dies entspricht einem Druckabfall von ungefähr 1 mbar innerhalb eines Tages. Einige Methoden zur Bestimmung der Gasdichtheit waren in der Vergangenheit betrachtet worden. Diese Diplomarbeit beschäftigt sich mit einer innovativen Möglichkeit. Die Gasverstärkung und folglich die Signale sind eine Funktion der Gasdichte. Der Test auf Gasdichtheit durch die Kammern selbst ermöglicht eine Bestimmung der Leckrate mit einer Empfindlichkeit besser als 10^{-4} innerhalb eines Tages. Die Grundlagen dieser Methode werden behandelt und demonstriert. Auch die Qualitätskontrolle von Einzelrohren kann durchgeführt werden. Die Methode erlaubt eine einfache Serienkontrolle im integrierten Test anderer Kammereigenschaften.

Abstract

ATLAS is a general-purpose experiment for the future Large Hadron Collider (LHC) at CERN. Its Muon Spectrometer will require $\sim 5500\,\mathrm{m}^2$ of precision tracking chambers to measure the muon tracks along a spectrometer arm of 5 m to 15 m length, embedded in a magnetic field of $\sim 0.5\,\mathrm{T}$. The precision tracking devices in the Muon System will be high pressure drift tubes (MDTs). Approximately 370,000 MDTs will be assembled into ~ 1200 drift chambers.

The performance of the MDT chambers is very much dependent on the mechanical quality of the chambers. The uniformity and stability of the performance can only be assured providing very high quality control during production. Gas tightness, high-voltage behaviour and dark currents are global parameters which are common to gas detectors. For all chambers, they will be tested immediately after the chamber assembly at every production site. Functional tests, for example radioactive source scans and cosmic-ray runs, will be performed in order to establish detailed performance maps.

One major issue of the quality control, the gas tightness, is the topic of this thesis. The gas pressure inside the tubes will be 3 bar, the drift gas will be Ar/CO_2 93/7. The high spatial resolution made it necessary to define the maximum allowed leak rate for MDT chambers to $2 * 10^{-8} \frac{bar\ l}{s}$. This is equivalent to a pressure drop of about 1 mbar for MDT chambers within one day at the given working point. Several methods had been considered in the past. This thesis deals with an innovative method. The gas gain and hence the signals are a strong function of the gas density. The test on the gas tightness using the tubes itself as sensitive devices makes it possible to determine the leak rate with a sensitivity better than 10^{-4} within one day. The principle of this method will be discussed and demonstrated. Also the quality control of single tubes can be realized with it. The method allows easy-to-use series controls with integrated test of other chamber properties.

Acknowledgements

Chris Fabjan did a great job guiding me through the work during my diploma thesis. His motivation showed me the way out whenever I felt stuck. I say thank you to him and his wife Monika for making the start in a foreign region so easy.
In the beginning it was Michael Treichel who helped me getting started at CERN and in my field of research. Martin Woudstra never hesitated to discuss subjects of physics with me. Together we spent of lot of days in DATCHA screwing datamizers and looking at the oscilloscope.
Having so many nice colleagues around made me feel comfortable here. Not only during work, also outside CERN I had a great time with Martin, Sophie, Edda, Werner and Helmut. I want to tell you that I am happy I have met you and hope we will have some more fun together.
Sometimes I went back to Vienna and the friends there told me that they did not forget me, although they never visited me in the beautiful french and swiss region. At least meeting them in Vienna was just like having holidays. Keeping e-mail contact with Bernhard was a great habit. Reading his endless reports of life in Vienna was a welcome distraction.
With Hemma I had ups and downs during the long time we spent together. However, from the beginning of our friendship until now, most of the time was a lot of fun. I wish our friendship will never end.
Whenever my Brüderchen took the chance to visit me, and he did it twice, I enjoyed it at lot. Traute and Wolfi accepted - as they always do - my sudden ideas and future plans. For their understanding and their great support I am very grateful.
Thanks to you all, Adrian.

Contents

Chapter 1

From LHC to the MUON spectrometer

1.1 Introduction

The next generation of high-energy physics research facilities has to operate in the TeV range in order to address important new issues of elementary particle physics (see Section 1.3). This chapter gives an introduction to the **L**arge **H**adron **C**ollider (LHC). This accelerator will allow to explore particle physics up to energies that dominated the universe just 10^{-17} s after the "Big Bang" when the temperature was about 10^{16} K. We will discuss the physics potential of the collider and focus afterwards on its impact on the design of the ATLAS experiment and – in greater detail – its Muon System.

1.2 The LHC

1.2.1 Design Parameters of the LHC

Already in the beginning of the 1980's, people at CERN started to think about testing the standard model beyond LEP energies. The LEP machine (e^+-e^-) has worked around the Z resonance ($M_Z = 91.187\,\mathrm{GeV}/c^2$) and is presently upgraded to LEP2 with a maximum centre-of-mass energy $\sqrt{s}$ of $\geq 200\,\mathrm{GeV}$. This value of $\sqrt{s}$ is the practical limit achievable with a circular electron accelerator in the 27 km circumference LEP tunnel due to the rapid increase of synchrotron radiation loss with energy. The large mass of hadrons with respect to electrons has the advantage that less energy is lost due to this effect. The main disadvantage of a hadron collider is the compositeness of the hadron. This means that the available energy of the hadron is distributed over the individual constituents (quarks and gluons). Considering the above arguments and given that a new collider at CERN has to match the existing LEP tunnel, the LHC was designed. It is planned to be operational in the year 2005. The LHC will be a p-p collider with a centre-of-mass energy $\sqrt{s}$ of

$2 \times 7 = 14\,\text{TeV}$ and a design luminosity of $\mathcal{L} = 10^{34}\,\text{cm}^{-2}\text{s}^{-1}$. Apart from accelerating protons, it will be possible to use the LHC with Pb-Pb ions at a centre-of-mass energy in the PeV range. The LHC will consist of two separate beam lines (with counter-rotating beams) which will be installed in the existing LEP tunnel and will be filled with 0.45 TeV protons delivered from the **S**uper **P**roton **S**ynchrotron (SPS) and its pre-accelerators (see Figure 1.1).

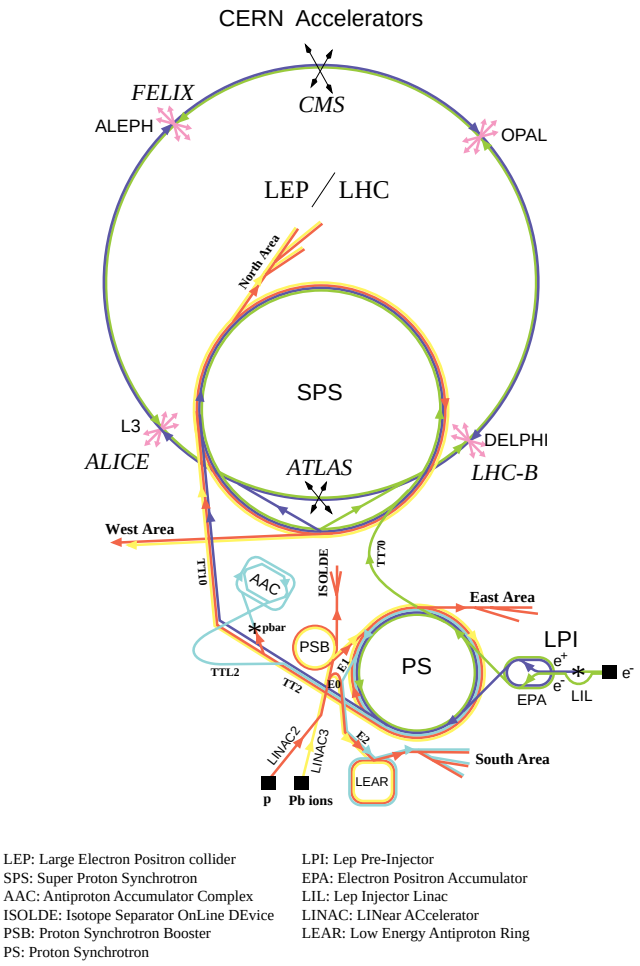

Figure 1.1: *Schematic view of the CERN accelerator complex.*

The beam line will be occupied with super-conducting NbTi bending magnets, quadrupoles for the beam optics and accelerating cavities. These magnets will house two separated beam lines with opposite magnetic fields of 8.4 T strength. The 1232 dipole magnets which are foreseen along the beam line will be $\sim 14.6\,\text{m}$ long.

At the interaction points, the bunches will have a transverse radius of $15\,\mu\text{m}$ and the length of the bunch will be 30 cm. This means that the position of the vertex will have a rather large spread along the beam direction, the effective spread of the distribution of the vertex position is expected to be 5.5 cm (r.m.s) along the beam direction.

1.2.2 Particle Production Rates

In Figure 1.2 some important production cross-sections and interaction rates are shown as a function of the centre-of-mass energy $\sqrt{s}$. The total cross-section is estimated to be between 90 and 130 mb. This means that on average there will be about 20 interactions in the centre of the detectors per bunch crossing (i.e. every 25 ns) at full luminosity $\mathcal{L} = 10^{34}\,\mathrm{cm}^{-2}\mathrm{s}^{-1}$. Small angle elastic and inelastic proton-proton scattering will be the most numerous and will dominate the 20 underlying events per bunch crossing. The total integrated luminosity is expected to be 10^5 events/(pb $\times$ year).

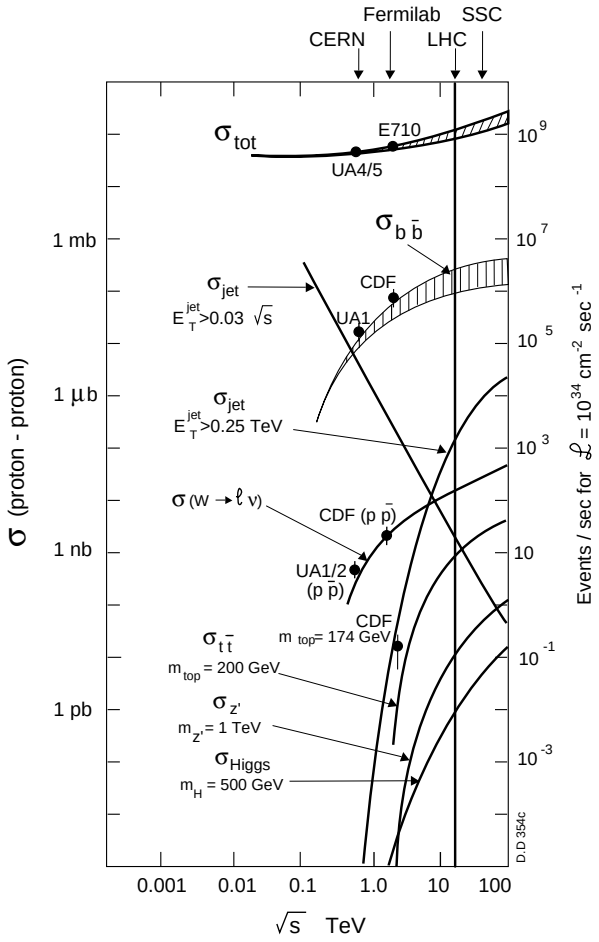

Figure 1.2: *The cross-section of some characteristic processes [1]. The centre-of-mass energy of LHC is indicated at the top. At $\sqrt{s} = 14$ TeV the production of the Higgs is eleven orders of magnitude less frequent than small angle p-p scattering.*

1.3 Physics at LHC and Detector Requirements

One of the main goals of LHC is to study the actual mechanism for symmetry breaking in the electroweak sector (SU(2) $\times$ U(1)) of the **S**tandard **M**odel (SM). This phenomenon

is associated with the nature of the Higgs mechanism, the existence of the Higgs particle and the behaviour of the cross-sections involving the gauge bosons, $W^{\pm}$ and Z. The LHC is designed to explore all the range of "allowed" Higgs masses and more, hence the planned experiments either must find the Higgs boson or contradict the Standard Model. In this section we will discuss the Higgs production and decay channels for the whole range of Higgs masses.

At the LHC heavy fermions (bottom and top-quarks) will be produced in large quantities. Hence, beside the Higgs search also B physics and the study of top-quark production and decay will be interesting issues for the LHC physics programme.

All these examples for LHC physics are used as benchmark processes for the detector design. In this Section we discuss briefly these benchmark processes and show their impact on the design of the various LHC detectors.

1.3.1 The Standard Model Higgs Boson

The most prominent benchmark processes for the detector design at LHC are the different Higgs-decay channels for the Higgs-mass range from $80\,\mathrm{GeV}/c^2$ to $1\,\mathrm{TeV}/c^2$. The Higgs coupling to other particles is proportional to their masses. It couples to quarks and leptons of mass m_f with a strength $g\frac{m_\mathrm{f}}{2M_\mathrm{W}}$. If the Higgs mass is very large, the couplings of the Higgs to itself and to longitudinally polarised gauge bosons become large. Requiring that these couplings remain weak enough that perturbation theory is applicable implies that $M_\mathrm{H} \leq 1\,\mathrm{TeV}/c^2$. This becomes more clear by pointing out that the width of the Higgs boson is proportional to the cube of its mass (for $M_\mathrm{H} > 2M_\mathrm{Z}$) and that a boson of mass $1\,\mathrm{TeV}/c^2$ has a width of Γ_H of $500\,\mathrm{GeV}/c^2$ (see Figure 1.3) and hence dissolves into the background. At the moment the lower limit of the Higgs mass is $94.1\,\mathrm{GeV}/c^2$ [2] (at 95 % confidence level) since it has not been discovered yet with LEP2. The Standard Model prefers a value for the Higgs mass close to $100\,\mathrm{GeV}/c^2$. In the **M**inimal **S**uper-symmetric extension of the **S**tandard **M**odel (MSSM) a family of Higgs bosons is predicted with an upper limit for the lightest super-symmetric Higgs boson of $130\,\mathrm{GeV}/c^2$.

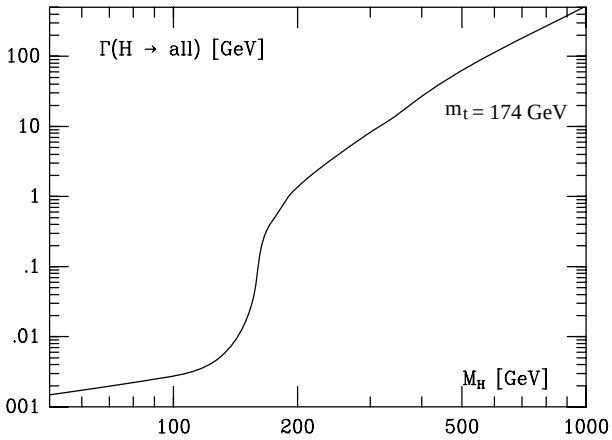

Figure 1.3: *Total Higgs width* Γ_H *as a function of* M_H.

Higgs Production

The production cross-section of the Higgs is typically 1 pb, assuming the Higgs mass with $500\,\mathrm{GeV}/c^2$. This corresponds to 10^5 produced Higgs bosons per year (or 1 Higgs boson every 2 minutes). The cross-section increases rapidly for a low-mass Higgs. The most dominant production mechanisms are the gluon-gluon fusion and the WW(ZZ) fusion. Figure 1.4 shows the Feynman-Diagrams for these two processes. Less important production channels are $t\bar{t}$ fusion and W or Z Bremsstrahlung [1].

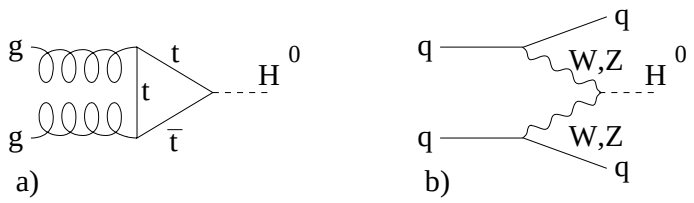

Figure 1.4: *The most dominant channels for the Higgs production: a) gluon-gluon fusion; b)* WW *and* ZZ *fusion.*

Higgs Decay

In Figure 1.5 the branching ratios are shown for Higgs masses between 50 and $600\,\mathrm{GeV}/c^2$. Only a few decay channels of the Higgs boson are accessible to experimental observation since the decay channels have either small branching ratios, or they are obscured by a large background of events. Statistics will be the limiting factor in the detection of the Higgs boson, in particular for Higgs masses approaching $1\,\mathrm{TeV}/c^2$.

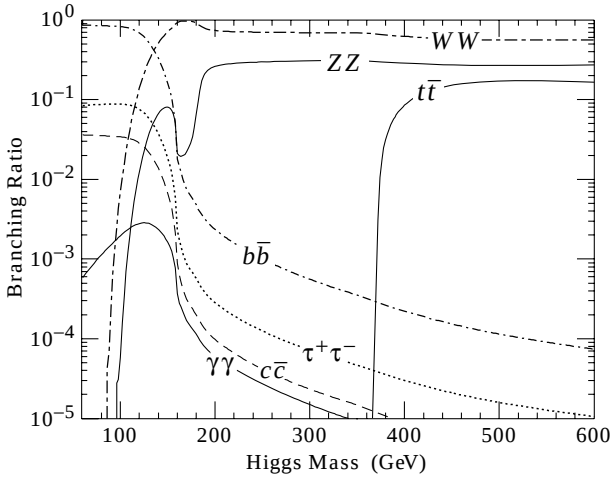

Figure 1.5: *Branching ratios of the Higgs.*

- **Low-Mass Higgs Boson ($M_\mathrm{H} < 120\,\mathrm{GeV}/c^2$):**
  Below the WW or ZZ threshold ($M_\mathrm{H} < 2M_\mathrm{Z}$), the dominant decay into the heaviest accessible pair of quarks ($\mathrm{H} \rightarrow \mathrm{b\bar{b}}$) is swamped by the QCD background (the direct $\mathrm{b\bar{b}}$

cross-section is very high, see Figure 1.2). Another decay channel in this regime can be the decay $WH \rightarrow l\nu\gamma\gamma$, which has almost no background, but unfortunately the production rate is very small. The third decay channel $H \rightarrow \gamma\gamma$ suffers an enormous background from $q\bar{q} \rightarrow \gamma\gamma$, $gg \rightarrow \gamma\gamma$, $gq \rightarrow q\gamma\gamma$ and $Z \rightarrow e^+e^-$ processes, where the jets or $e^\pm$ fake a γ. These backgrounds can be reduced with excellent photon resolution and excellent γ/jet and $\gamma/e^\pm$ discrimination. Hence an electromagnetic calorimetry with excellent performance is required.

- **Intermediate-Mass Higgs Boson ($120\,\mathrm{GeV}/c^2 < M_H < 800\,\mathrm{GeV}/c^2$):**
  In this mass region the decay $H \rightarrow ZZ^{(*)} \rightarrow l^+l^-l^+l^-$ provides a very clean signature of the Higgs boson. For the range $M_H < 2M_Z$ one of the two Z bosons is virtual. For a Higgs mass of $150\,\mathrm{GeV}/c^2$ one expects ~ 550 such events per year. The four leptons have a high transverse momentum ($5\,\mathrm{GeV}/c < p_T < 50\,\mathrm{GeV}/c$). The natural Higgs width Γ_H is small in this regime (see Figure 1.3) and the background is mainly coming from prompt muons, decay muons, hadronic punch-through, neutrons and muon induced electromagnetic secondaries. To achieve a good acceptance for such kind of events, the geometrical and kinematic acceptance for leptons has to be maximised, the significance of the signal will depend on the four-lepton mass resolution. Hence a good lepton energy and momentum resolution at the level of 1 % is necessary. For large Higgs boson masses the Higgs width increases rapidly and the signal will be rate limited, hence the accelerator luminosity becomes more important than the detector performance.

- **Heavy-Mass Higgs Boson ($M_H > 800\,\mathrm{GeV}/c^2$):**
  For a heavy Higgs boson the channel $H \rightarrow ZZ \rightarrow l^+l^-\nu\bar{\nu}$ becomes six times more frequent than $H \rightarrow ZZ \rightarrow l^+l^-l^+l^-$ and can be detected with the measurements of two high-p_T leptons and a high missing E_T due to the escaping neutrinos. Also the channels $H \rightarrow WW, ZZ \rightarrow l^\pm\nu 2\mathrm{jets}, 2l^\pm 2\mathrm{jets}$ provide promising signatures for a heavy Higgs boson.

1.3.2 Experiments

In order to exploit the full discovery potential of LHC two general-purpose proton-proton experiments (ATLAS and CMS) and two specialised experiments (ALICE and LHCb) will be installed at the beam crossings (see Figure 1.1).

The main difference between the two general-purpose experiments lies in their magnet configurations for muon spectroscopy. The choice of the magnet system strongly influences the geometry of the detector.

- **ATLAS:**
  The ATLAS (**A** **T**oroidal **L**HC **A**pparatu**S**) experiment is characterised by the following magnet configuration: A super-conducting solenoid will be installed around the Inner-Detector cavity and large super-conducting air-core toroids consisting of independent coils will be arranged outside the calorimetry. This concept offers almost no

constraints on calorimetry and Inner Detector allowing noncompromised technological solutions and a high-resolution, large-acceptance and robust Muon Spectrometer with excellent stand-alone capabilities.

ATLAS will be 22 m high, 44 m long, and will have a weight of $\sim$ 6000 tons.

The ATLAS experiment will be explained in greater detail in the next section.

- **CMS:**
  The CMS (**C**ompact **M**uon **S**olenoid) experiment is based on a single, large, superconducting solenoidal magnet (14 m long and 3 m inner radius) generating a uniform magnetic field of 4 T. The choice of a strong field leads to a compact design for the Muon Spectrometer without compromising the momentum resolution up to pseudo-rapidities[1] of 2.5.

  CMS will be 14 m high, 20 m long, and will have a weight of $\sim$ 12,000 tons. For more detailed information see [3].

- **ALICE:**
  It is planned to convert the existing L3 detector into the ALICE (**A** **L**arge **I**on **C**ollider **E**xperiment) experiment to investigate Pb-Pb collisions. This heavy-ion detector will be used to study physics of strongly interacting matter at extreme energy densities. For more detailed information see [4].

- **LHCb:**
  This dedicated B physics experiment at the LHC will be built in the DELPHI pit. It is an open-geometry forward collider detector which is designed to fully exploit the B physics potential of the LHC. The large Lorentz boost of accepted B-mesons allows precise decay-time measurements, which are complemented by excellent particle identification and efficient muon triggers. For more detailed information see [5].

[1] The pseudo-rapidity η is defined as $\eta \equiv -\ln\tan(\theta/2)$, where θ is the polar angle with respect to the beam line.

1.4 The ATLAS Detector

The ATLAS collaboration proposes to build a general-purpose proton-proton detector which is designed to exploit the full discovery potential of LHC [6]. The collaboration submitted a Letter of Intent in 1992, a Technical Proposal in 1994 and **T**echnical **D**esign **R**eports (TDRs) for each subsystem including most of the final specifications. Construction started in 1998 and the experiment should be ready for the start of LHC in 2005. Figure 1.6 shows a 3D view of the final design of the whole ATLAS experiment.

As pointed out in Section 1.3, many of the interesting physics questions at the LHC require high luminosity. A variety of signatures is important to achieve robust and redundant physics measurements with the ability of internal cross checks. The goal to exploit the full physics potential of LHC and the requirements introduced in Section 1.3 lead to the following basic design considerations:

- very good electromagnetic calorimetry for electron and photon identification and measurements, complemented by hermetic jet and missing E_{T} calorimetry;
- efficient tracking at high luminosity for lepton-momentum measurements, for b-quark tagging, and for enhanced electron and photon identification, as well as τ and heavy-flavor vertexing and reconstruction capability of some B-decay final-states at lower luminosity;
- stand-alone, precision muon-momentum measurements up to highest luminosity, and very low-p_{T} trigger capability at low luminosity;
- large acceptance and maximum η coverage.

1.4.1 The Inner Detector

The ATLAS Inner Detector is shown in Figure 1.7. It combines high-resolution detectors at inner radii with continuous tracking elements at outer radii, all contained in a solenoidal magnet with a central field of 2 T. For more detailed information see [7].

The silicon-pixel vertex-detector consists of three barrel layers of 140 million pixels (each 50 μm in r-φ direction and 300 μm in the direction along the beam line) and four disks on each side between radii of 11 cm and 14 cm aiming for a point resolution of $\sigma_{r,\varphi} = 12\,\mu$m and $\sigma_z = 60\,\mu$m. This high resolution allows to reconstruct the track origin to find secondary decay vertices. The readout chips must withstand over 300 kGy of ionising radiation and over $5 \cdot 10^{14}$ neutrons/cm^2 in ten years of operation.

The silicon strip detectors – **S**emi **C**onductor **T**racker (SCT) – with a pitch of 80 μm are mounted in four barrel layers at radii of 30, 37.3, 44.7 and 52 cm in order to provide four precision measurements per track in the intermediate radial range, contributing to the measurement of momentum, impact parameter and vertex position. The spatial resolution will be $\sigma_{r,\varphi} = 18\,\mu$m and $\sigma_z = 580\,\mu$m.

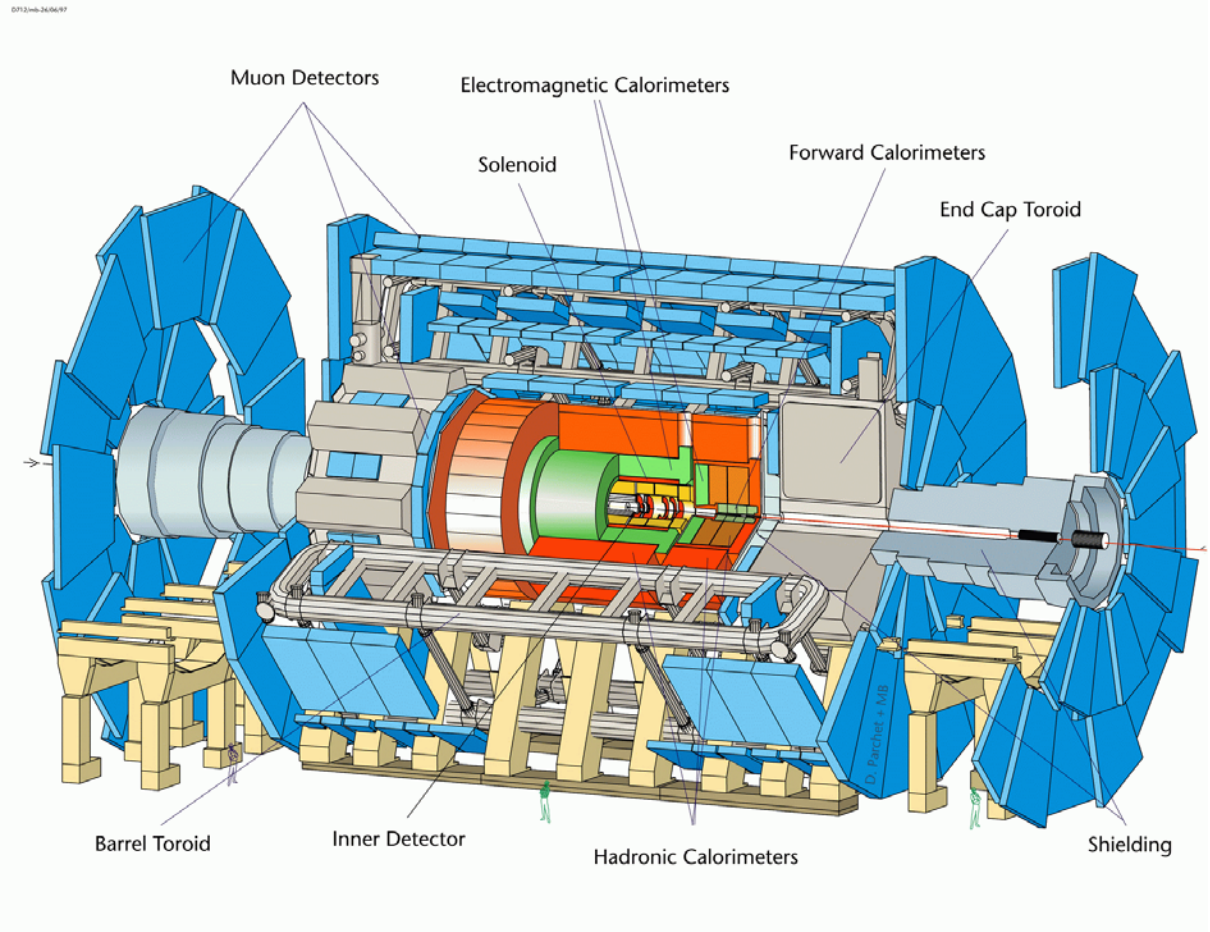

Figure 1.6: *3D view of the ATLAS detector.*

The **T**ransition **R**adiation **T**racker (TRT) consists of 420,000 proportional drift tubes with a diameter of 4 mm. It is divided into a barrel part and several forward wheels. The detector is operated with a $Xe/CF_4/CO_2$ gas mixture optimised for the detection of X-rays created as transition radiation in stacks of thin radiators between the tubes. The single-wire resolution will be 170 μm and the efficiency will be $> 50\,\%$ even for the highest rates (15 MHz). Two different discriminator thresholds will be used to distinguish between tracking hits (only lower threshold) and transition-radiation hits (both thresholds).

1.4.2 Calorimetry

The ATLAS calorimetry is shown in Figure 1.8. It consists of an electromagnetic calorimeter and a hadronic calorimeter. A barrel cryostat around the inner cavity contains the barrel electromagnetic **L**iquid **Ar**gon (LAr) calorimeter and the coil of the solenoid magnet. Two end-cap cryostats enclose the electromagnetic and hadronic end-cap calorimeters as well as the integrated forward calorimeter. For more detailed information see [8].

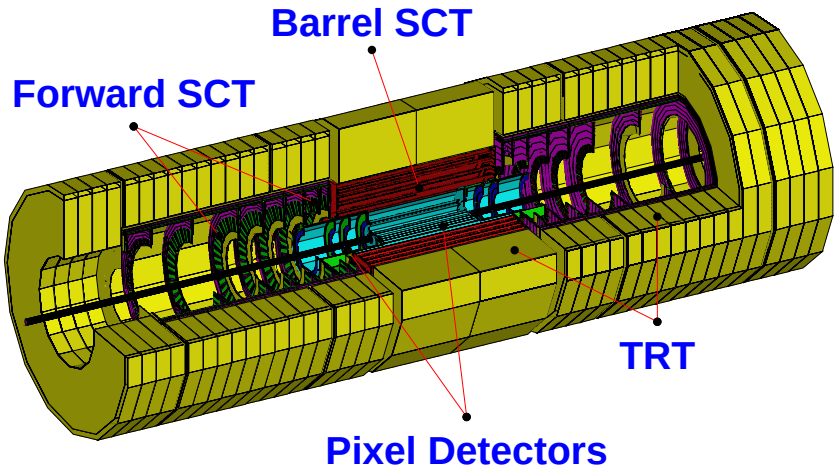

Figure 1.7: *Atlas Inner Detector consisting of a pixel detector system, the SCT and the TRT. The whole Inner Detector has a length of* 6.8 m *and a radius of* 1.15 m.

- **The Electromagnetic Calorimeter:**
  The electromagnetic calorimeter is a lead-LAr detector with accordion shaped Kapton electrodes and lead absorber plates over its full coverage[2]. The LAr sampling technique is radiation resistant and provides long-term stability of the detector response, excellent hermiticity, good energy resolutions, and relatively easy detector calibration. The total thickness of the electromagnetic calorimeter is $> 24\,X_0$ in the barrel part and $> 26\,X_0$ in the forward region. The segmentation of the calorimeter will be $\Delta\eta \times \Delta\varphi \approx 0.025 \times 0.025$, aiming for an energy resolution of $\Delta E/E = 10\,\%/\sqrt{E} \oplus 1\,\%$ (E in GeV). The energy-scale precision will be 0.1 % and the measurement resolution of the shower direction in θ will be $\sim 50\,\text{mrad}/\sqrt{E}$ (E in GeV).

- **The Hadronic Calorimeter:**
  The barrel hadronic calorimeter will have an inner radius of 2.28 m and an outer radius of 4.23 m. The hadronic calorimeter uses different techniques and devices as best suited for the different requirements and the radiation environment. The total thickness is 11 interaction lengths λ at $\eta = 0$, including $1.5\,\lambda$ of the outer support. In the range of $|\eta| < 1.6$ a sampling calorimeter is used with iron as absorber material and scintillating tiles (3 mm thick) as active material (TILE Calorimeter). The signals produced on both sides of the scintillating tiles are read out by wavelength-shifting fibres into two separate photo-multipliers. The resulting segmentation of the hadronic calorimeter will be $\Delta\eta \times \Delta\varphi \approx 0.1 \times 0.1$. In the range of $1.5 < |\eta| < 4.9$ a hadronic LAr calorimeter is used. The end-cap hadronic calorimeter extends up to $|\eta| < 3.2$ and is a copper-LAr detector with parallel plate geometry. The high-density forward calorimeter covers the region of $3.2 < |\eta| < 4.9$ with the front face about 5 m from the interaction point (high level of radiation). The detector is based on rods filled with LAr in a copper and tungsten matrix. The expected energy resolution for the hadronic calorimeter is $\Delta E/E = 50\,\%/\sqrt{E} \oplus 3\,\%$ for $|\eta| < 3$ and $\Delta E/E = 100\,\%/\sqrt{E} \oplus 10\,\%$ for $3 < |\eta| < 4.9$.

[2]Barrel part: $|\eta| < 1.475$, end-cap parts: $1.375 < |\eta| < 3.2$.

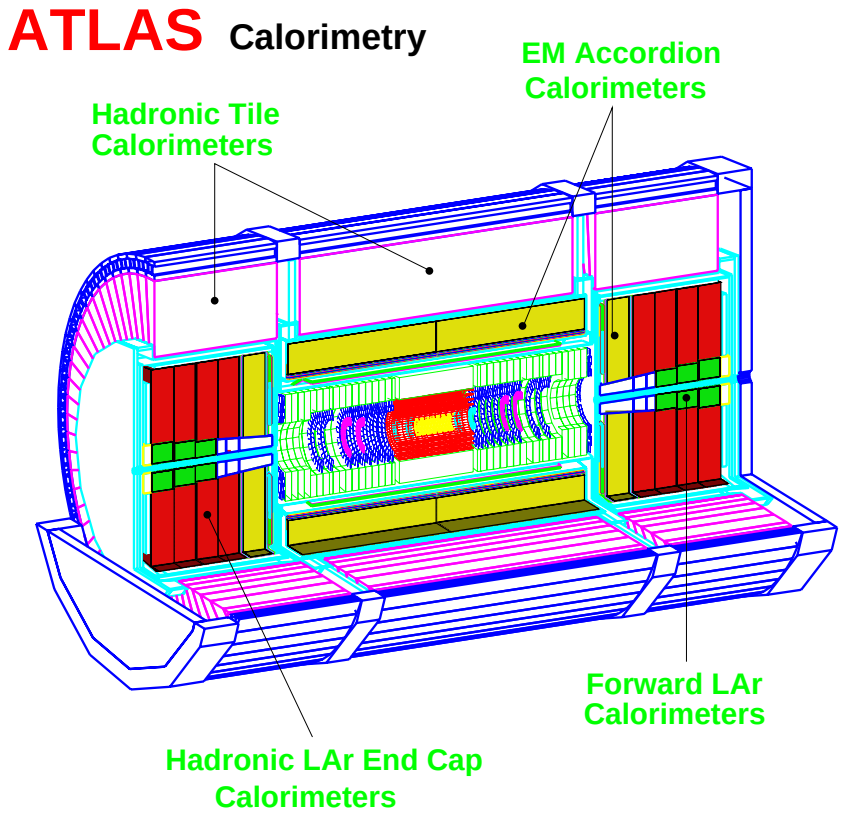

Figure 1.8: *Layout of the ATLAS calorimetry system.*

1.4.3 The Muon Spectrometer

The Muon Spectrometer dominates the size of the ATLAS experiment with its outer diameter of $\sim 22\,\text{m}$. Figures 1.9 and 1.10 show two cuts through the Muon Spectrometer.

The ATLAS Muon Spectrometer is based on the magnetic deflection of muon tracks in a system of three large super-conducting air-core toroid magnets instrumented with separate-function trigger and high-precision tracking chambers. The design and performance of the Muon Spectrometer must satisfy the following requirements:

- the largest possible discovery reach for expected and unexpected new physics, with minimal systematic biases;
- good discrimination against high levels of charged and neutral particle background from minimum-bias events and radiation;
- safe and reliable operation in difficult environmental conditions for the anticipated lifetime of the LHC.

The discovery potential of the spectrometer has been optimised on the basis of selected benchmark processes.

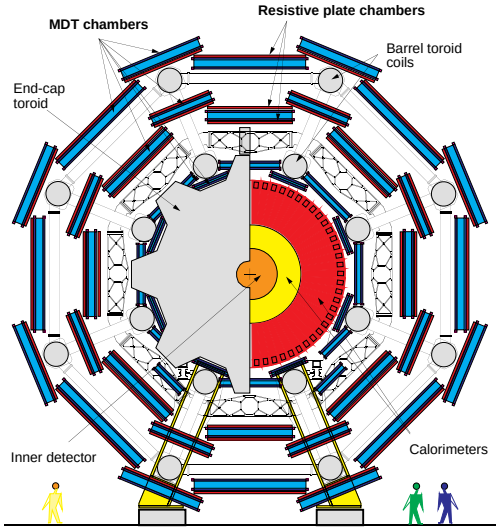

Figure 1.9: *Transverse view of the ATLAS Muon Spectrometer.*

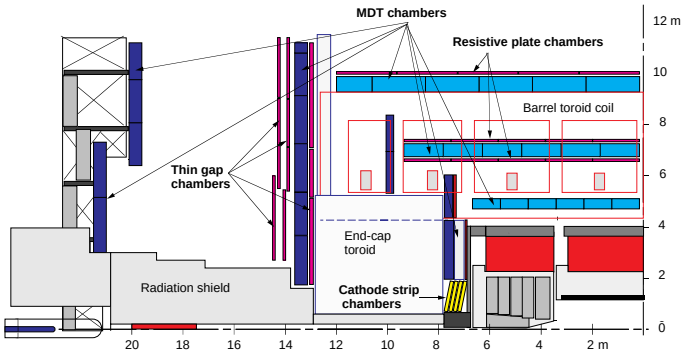

Figure 1.10: *Side view of one quadrant of the ATLAS experiment.*

Based on the discussion from Section 1.3 the important parameters that need to be optimised for maximum physics reach are:

- Resolution: momentum and mass resolutions at the level of 1 % are essential for the reconstruction of narrow two- or four-muon final states on top of high background levels, such as the intermediate-mass Higgs, and for reliable charge identification. A transverse momentum resolution that is constant over the full rapidity range is desirable.
- "Second coordinate" measurement: a measurement of muon tracks in the non-bending projections with an r.m.s spatial resolution of 5–10 mm is required for safe track reconstruction and reliable momentum determination.
- Rapidity coverage of track reconstruction: all physics channels profit from a pseudo-rapidity coverage up to $|\eta| \approx 3$ and good hermeticity, in particular rare high-mass processes.
- Trigger selectivity: transverse momentum thresholds of 10–20 GeV/c are adequate for high-mass states, which will be in the focus of LHC physics at nominal luminosity. Lower thresholds of $p_{\mathrm{T}} \approx 5\,\mathrm{GeV}/c$ are required for CP violation and beauty physics.
- Trigger coverage: adequate trigger efficiencies can be obtained with a pseudo-rapidity coverage smaller than that of the precision chambers. The actual requirements are mostly determined by processes at the opposite ends of the LHC mass scale: the need for good acceptance for rare high-mass Higgs particles, and the need for very high statistics to study small rate asymmetries due to CP violation in the B sector. A trigger coverage of $|\eta| < 2.4$ is found to be sufficient.
- Bunch-crossing identification: the LHC bunch-crossing interval of 25 ns sets the scale for the required time resolution of the first-level trigger system.

Achieving a resolution $\Delta p_{\mathrm{T}}/p_{\mathrm{T}} \approx 10\,\%$ for $p_{\mathrm{T}} = 1\,\mathrm{TeV}/c$ dictates the combination of the bending power in the central rapidity region, and of the precision with which the muon instrumentation must measure the sagitta of the particles.

Magnet System

The magnet system consists of three air-core super-conducting toroids with an open structure to minimise the contribution of multiple scattering to the momentum resolution. The toroidal design of the magnet system made it possible to provide a high-resolution, large-acceptance and robust stand-alone Muon Spectrometer. A combined optimisation of the magnet-field strength and its radius, constrained by magnet-fabrication costs and by space limitations in the experimental cavern, led to the air-core toroid magnet configuration providing a bending power at $\varphi = 0$ of $\int B\,\mathrm{d}l = 2\,\mathrm{Tm}$ at $\eta = 0$ up to $\int B\,\mathrm{d}l = 9\,\mathrm{Tm}$ at $|\eta| = 2.8$ (see Figure 1.12, the integral is calculated from the inner muon station to the outer muon station). The average toroidal magnetic field will be $\sim 0.5\,\mathrm{T}$. A big advantage of the toroidal magnetic field is the fact that the bending power increases with higher pseudo-rapidities.

The barrel toroid extends over a length of 25 m, with an inner bore of 9.4 m and an outer diameter of 20.1 m. The two end-cap toroids are inserted in the barrel at each end. They have a length of 5 m, an inner bore of 1.64 m and an outer diameter of 10.7 m. Each toroid consists of eight flat coils assembled radially and symmetrically around the beam axis. The barrel-toroid coils are contained in individual cryostats, whereas the eight end-cap toroid-coils are assembled in a single, large cryostat. Figure 1.11 shows a 3D view of the muon magnet system.

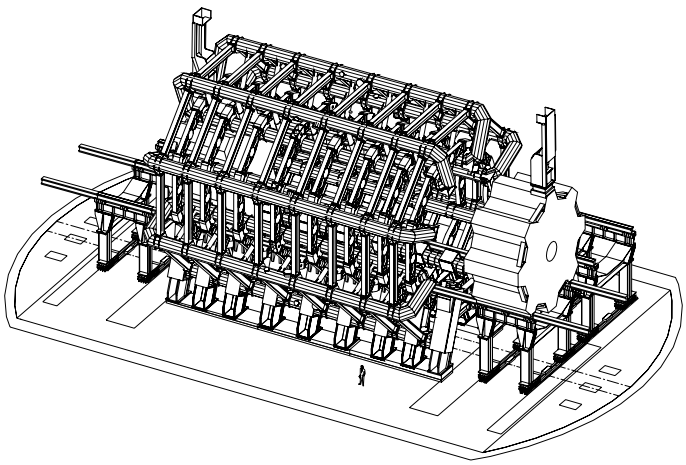

Figure 1.11: *3D view of the super-conducting air-core toroid magnet system.*

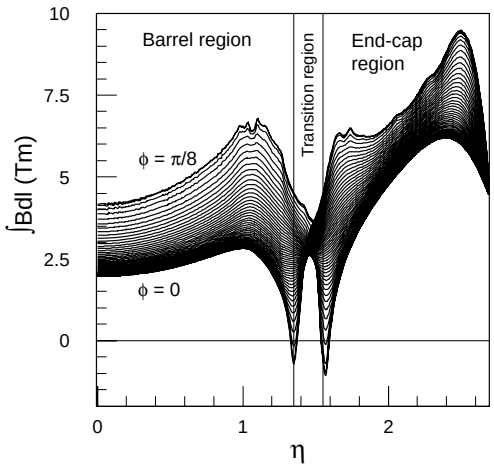

Figure 1.12: *Toroid bending power $\int B\,\mathrm{d}l$ of the azimuthal field component as a function of η.*

Muon Instrumentation

The ATLAS Muon Spectrometer will measure the trajectories of particles at three stations of chambers.

In the barrel ($|\eta| < 1$) they will be arranged in three cylinders concentric with the beam axis at radii of about 5 m, 7.5 m and 10 m. In this η-region the particles are measured near the inner and outer field boundaries, and inside the field volume, in order to determine the momentum from the sagitta.

The end-cap chambers will cover the pseudo-rapidity range $1 < |\eta| < 2.7$ and are arranged in four disks at distances of 7 m, 10 m, 14 m and 21–23 m from the interaction point. In the forward region, for $|\eta| > 1.4$, the magnet cryostats do not allow the positioning of chambers inside the field volume. Instead, the chambers are arranged to determine the momentum with the best possible resolution from a point-angle measurement.

The ATLAS Muon Spectrometer consists of four different chamber technologies:

- **Precision Chambers:**
  For the precision measurement of muon tracks in the principal bending direction of the magnetic field, **M**onitored **D**rift **T**ube (MDT) chambers are used except in the innermost ring of the end-cap inner-station ($2 < |\eta| < 2.7$), where particle fluxes are highest. The layout of the MDT chambers will be explained in Section 1.5.
  In the innermost ring of the end-cap inner-station **C**athode **S**trip **C**hamber**s** (CSCs) are employed (see Figure 1.10). The CSCs are multi-wire proportional chambers with cathode strip readout and with a symmetric cell in which the anode-cathode spacing is equal to the anode-wire pitch. A spatial resolution of 60 μm (r.m.s) has been measured. A transverse coordinate is obtained from the strips parallel to the anode wires, which form the second cathode of the chamber.

- **Trigger Chambers:**
  These chambers will provide the trigger function, the bunch-crossing identification and the measurement of the "second coordinate" (coordinate along the magnetic field line). In the barrel this information is provided by three stations of **R**esistive **P**late **C**hamber**s** (RPCs). They are located on both sides of the middle MDT station, and either directly above or directly below the outer MDT station. These chambers are gaseous parallel-plate chambers with a typical space-time resolution of 1 cm $\times$ 1 ns. Each chamber is made of two rectangular detector layers, each one read out by two orthogonal series of pick-up strips: The η-strips are parallel to the MDT wires and provide the bending view of the trigger detector; and the φ-strips, orthogonal to the MDT wires, provide the "second coordinate" measurement which is important for the off-line pattern recognition.
  In the end-caps, three stations of **T**hin **G**ap **C**hambers (TGCs), located near the middle MDT station will be installed. The TGCs have a structure similar to multi-wire proportional chambers, with the difference that the anode-wire pitch (1.8 mm) is larger than the cathode-anode distance (1.4 mm). Signals from the anode wires, arranged parallel to the MDT wires, provide the trigger information together with

readout strips arranged orthogonal to the wires, that also provide a measurement of the "second coordinate".

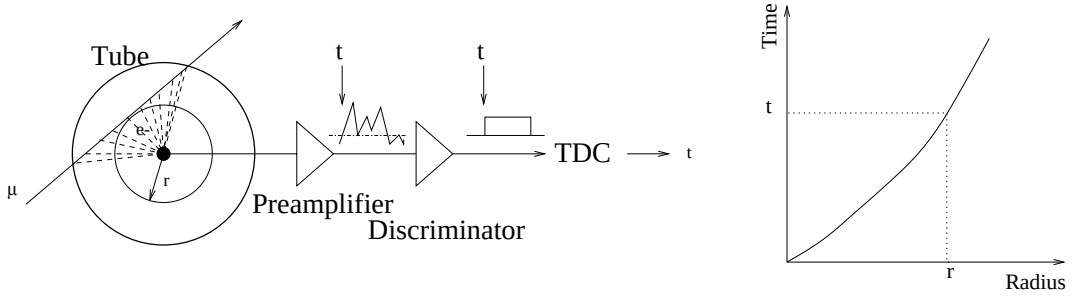

Figure 1.13: *Principle of the MDT operation. The electron-drift time is measured and converted to a distance via a space-time relationship (rt-relation).*

1.5 Muon Precision Drift Chambers

The sagittas of muon tracks are measured by precision chambers in an inner, middle and outer muon station (see also [9]). A muon with $p_{\mathrm{T}} = 1\,\mathrm{TeV}/c$ shows a sagitta of $\sim 500\,\mu$m in an average magnetic field of 0.5 T; thus a momentum resolution of 10 % requires a sagitta-measurement accuracy of $50\,\mu$m. The relative position of the muon chambers in the inner, middle and outer station will be monitored by an optical alignment system. The basic elements of these chambers are Aluminium[3] drift tubes (MDTs) with an outer diameter of 3 cm (wall thickness of $400\,\mu$m) and a $50\,\mu$m central wire (W/Re 97/3, gold-plated 3 % by weight) that is connected to positive high voltage.

A single tube accuracy of the track measurement of $70\,\mu$m is required for the needed sagitta-measurement accuracy. By increasing the pressure of the gas mixture, the main contribution to the spatial resolution, cluster position fluctuations and primary ionisation fluctuations, is decreased. The high pressure requires, that the construction of single tubes has to be cylindrical to ensure the mechanical stability.

1.5.1 The Principle of Operation

The principle of operation is shown in Figure 1.13. A muon crossing the MDT ionises the detector gas along its track, the electrons are drifting towards the wire in the electric field and are multiplied in an avalanche process close to the wire due to the high field (see Section 3.3). The movement of the electrons and ions induces a current on the wire that is read out at one end of the tube by a current sensitive preamplifier. After discriminating the signal, a **T**ime to **D**igital **C**onverter (TDC) stores the arrival time of the pulse, such measuring the drift time of the ionisation electrons. The drift time is then converted to a distance using the space-time relationship, which will be often referred to as "rt-relation" throughout this work. If the drift velocity depends only weakly on the electric field, the rt-relation is almost linear. Hence we call it a "linear" gas, otherwise we speak of "non-linear" drift gases. The rt-relation is obtained by a so-called auto-calibration procedure [10, 11]. The detailed analysis of the contributions to the spatial resolution that can be obtained

[3] ALUMAN-100, German DIN norm AlMn-DIN-1700.

with such a drift tube is discussed in [12].

The MDT chambers consist of two multilayers separated by a support structure. Each multilayer combines three[4] or four[5] layers of tubes (see Figure 1.14). The support structures provide accurate positioning of the two multilayers with respect to each other and mechanical integrity under effect of gravity and temperature. An X-ray Tomograph will be used to check the wire-position accuracy before the chambers are installed(see Section 2.1.The MDT in-plane alignment system will monitor the wire displacement[6] in the experiment with an accuracy of 10 μm or better (see Figure 1.14). The 1194 MDT chambers will cover an area of 5500 m^2. The total number of readout channels is 370,000.

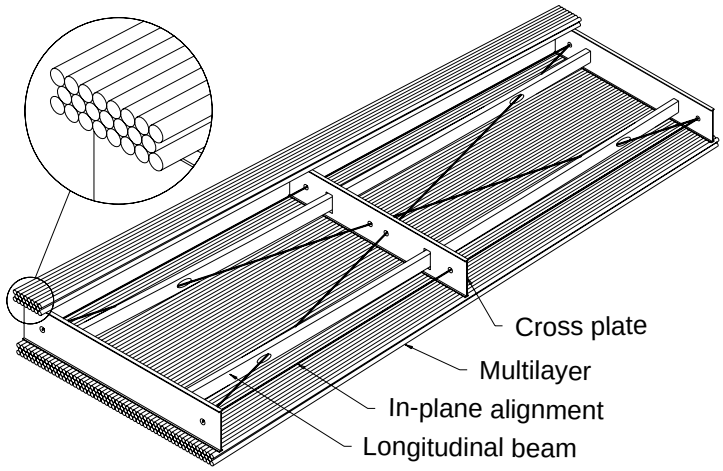

Figure 1.14: *Two multilayers of MDT tubes each consisting of three or four layers are glued to a support frame ("spacer structure") to form a chamber.*

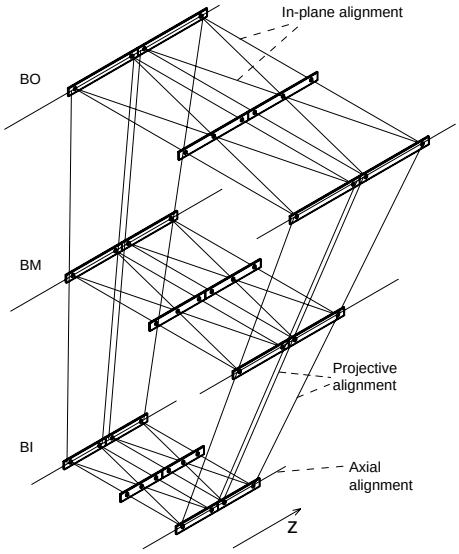

Figure 1.15: *The projective alignment system in the barrel region.*

1.5.2 The Projective Alignment System

The momentum measurement in the Muon Spectrometer will be a sagitta measurement in triplets of precision chambers. The level of accuracy is determined by the spatial resolution of the precision chambers as well as by the exact knowledge of the positions of the chambers with respect to each other. This information will be provided by the projective alignment system.

The arrangement of the light rays for the alignment of barrel towers is shown in Figure 1.15. In this projective layout, and in linear approximation, the correction to the

[4]In the middle and outer station.

[5]In the inner station.

[6]Such displacements are inferred from relative movements of the three cross-plates which are part of the chamber support structure.

measured sagitta of the muon trajectory is a function of six chamber-displacement parameters. Four laser rays monitored with two-dimensional optical sensors therefore provide for an over-constrained measurement of chamber movements. The projective monitoring is implemented in RASNIK technology [15].

In order to control the relative positioning of chamber stations inside each sector, the distance and the direction of the axial laser rays are monitored with silicon sensors mounted on a stiff reference frame.

The optical alignment system must measure the relative position of the inner, middle and outer muon station with an accuracy such that the maximum alignment contribution to the sagitta measurement is $< 30\,\mu$m.

Chapter 2

Quality Control

The properties of all MDTs and chambers will be tested for several times prior to installation. At the production sites the gas tightness and the tube functionality of individual tubes will be checked before assembly. For completed MDT chambers are tested for mechanical properties, gas tightness and R/O functionality including the on-chamber electronics like preamplifier and TDC cards. For chambers this will happen at the production sites before delivery and at CERN site shortly prior to installation in the UXA.

2.1 Quality Control Tasks on MDTs and Chambers

Industrially produced components are used to a large extent in all chamber types. Their quality will be continuously evaluated during the series production. Gas tightness, high-voltage behaviour, and dark currents are global performance parameters which are common to gas detectors. For all chamber types, they will be tested immediately after the chamber assembly, at every production site. Moreover, functional tests, for example radioactive source scans and cosmic-ray runs, will be performed.

- Gas tightness

  A possible method is to monitor pressure and temperature for a period of several days or weeks. For example, in a common tubes the maximum allowed leak rate of $2*10^{-8}$ bar l/s will translate into a pressure drop of about 1 mbar in one day at constant temperature. Another - more innovative - possibility for tests on gas tightness is the main topic of this thesis (see Chapter 3).

- High voltage

  Once all the front-end electronics is mounted, the high voltage is ramped up to the operating voltage of more than 3000 V. Dark current and count rates are monitored during this operation.

- Functionality tests

Pulse heights and shapes of signals from radioactive sources are used to test both the tube response and the functionality of the FE electronics.

- Mechanical properties

  The first readout test of the in-plane alignment system does not not only serve to check its functionality, but also yields a reference data set for later monitoring of deformations. It has to be performed under reproducible conditions: the chamber is horizontally suspended at three points and is filled with gas under the operating pressure, temperature and possibly strain profiles are measured and recorded. The precision of the mechanical assembly of MDT chambers is also verified by the X-ray Tomograph.

X-ray-Tomograph

A very elegant way to verify wire positions inside an assembled chamber makes use of the enhanced absorption of a fine, collinear X-ray beam in the tungsten wires as opposed to the aluminium of the tube walls and the gas. The main parts of the of the X-ray Tomograph are collimated X-ray sources, which can be moved across the chamber on a rail with precise position control, and an X-ray detector. The latter item depends on the scanning method employed:

1. 'Passive': The chamber is placed between the X-ray source and a scintillator, the count rate of which is recorded as a function of the source position. From the absorption peak positions in this 'shadowgram' the wire positions can be reconstructed. [13]

2. 'Active': If the chamber is operational, the response of the tubes themselves can be measured. This gives both, positive and negative peaks on a smooth background which is produced by X-ray conversions in the operating gas: the count rate is enhanced when secondaries are produced by X-rays hitting the wire of the connected tube, it is depleted when X-rays are absorbed in wires between the connected tube and the X-ray source. This method provides at the same time a functionality test. [14]

Scanning under two different beam angles with respect to the chamber plane provides a stereo measurement such that a two-dimensional map of wire positions can be reconstructed.

For the functionality tests, cosmic-ray exposures are an alternative to source scans.It is envisaged to store the chambers under pressure (3 bar), in order to avoid the entry of dust and other pollution.

2.2 Integrated Test

The fact, that the number of components for the muon spectrometer, about 370 000 tubes in 1200 chambers, and the list of individual specifications, which have to be tested, are

very large, requires very efficient procedures. The effort of time, manpower and additional hardware should be kept small. The integration of several tests within one procedure is one possibility to minimise the time needed for a quality control. An integrated way of testing the functionality of tubes, HV and FE electronics and the gas tightness is the topic of this thesis. The performance of the front-end electronics can be recorded while determing the gas tightness of the chambers.

The complex design and the specifications of the MDT chambers needs intensive quality control. In the beginning of this diploma thesis the task was the development of a design for an procedure testing all properties of MDT chambers. This includes functionality tests of the tube response, mechanical construction properties, tightness of the gas system and performance of the the on-chamber electronics. Tests on the mechanical properties will be done using the in-plane alignment system. Electronics performance and tube functionality can be studied by taking data of radioactive or cosmic irradiation. A single parameter, the gas tightness of individual chamber systems is not designed to be monitored during operation. This fact makes it even more important to measure and assure the gas tightness already before the final installation. Mechanical procedures like a manometer require several days to measure the gas tightness to a reasonable sensitivity. Also a certain mechanical effort in addition to the other tasks is needed. The evaluation of the gas gain method uses the hardware already provided for the performance tests of tube and electronics. The gas gain method proposed in this thesis is a way of testing the gas tightness integrating the other mentioned test issues. From the beginning of this thesis inventing a general performance test on MDT chambers the work was concentrated on the issue of the gas tightness as it seemed to be the most difficult task. An elegant and innovative method was tested for its behaviour and limits.

The specifications for the maximum leak rate of the MDT chambers are at such a low level, that long measurement times are necessary to achieve sufficient accuracy. In many cases methods are used, which are also dependent on the temperature. Topic of this thesis is a way of measuring the gas tightness with the following advantages.

- Temperature independent

  Since the gas density instead of the pressure is measured, temperature uncertainties of first order drop out. In special cases and only for single tube tests temperature monitoring is needed with an accuracy of 0.1 K.

- no additional hardware

  The needed hardware for the method proposed in this thesis is relatively small compared to using a differential manometer, mass spectrometer or gas sniffer. Used parts are similar to the ones designed for ATLAS itself.

- high sensitivity

  As shown in chapter 3.6 the smallest detectable leak rate is about $0.5 * 10^{-8} \frac{bar\ l}{s}$ in a measurement time of 24 hours.

Chapter 3

Gas Leak Tests

3.1 Requirements

In drift chambers, variations of the fundamental properties of the gas, such as pressure, temperature and composition, have important effects on the tracking precision. Drift velocity and gas gain are quite sensitive to the gas density. Also the diffusion of drifting electrons depends on the gas composition. Finally, the lifetime of the tubes, limited by the gradual formation of insulating deposits on the anode and cathode surfaces, is sensitive to the presence of certain chemicals. The gas system must guarantee a very high stability of the operating conditions, as well as a maximum control of pressure, temperature and composition of the gas. The gas density also affects the relation between drift distance and drift time by having impact on the mean free path between collisions. This is another major motivation for keeping the gas density and the gas composition constant.

The gas leakage of the MDTs is therefore an important parameter to assure stable conditions of the gas. Requirements were defined in the Muon Spectrometer TDR [15]. The specification of the maximum leak rate is $10^{-8}\frac{bar\ l}{s}$ for single tubes and two times this value for a MDT chamber, taking into account the additional on-chamber gas distribution system [16]. For one tube meter ($V_{tubemeter} = 0.146^2\pi 10 \approx 0.67l$) in a MDT chamber and its allowed leak rate one calculates $\Delta p_{max} \approx 2.6 mbar/meter_{tube}$ for a 24 hour time period. A summary of leak rates and $\frac{\Delta\rho}{\rho} = \frac{\Delta p}{p}$ for chambers of certain types is given in Table 3.1. Half the given specifications is valid for single tubes of the given chamber type.

Because of an allowed pressure drop less than 2 mbar ($\frac{\Delta p}{p} < 10^{-3}$) per day and a shortness in

chamber	Volume$_{tube}$ [l]	$\Delta p_{max}[mbar/day]$
BIS	1.14	1.5
BML	2.40	0.72
BOL	3.34	0.52

Table 3.1: allowed pressure drop in 24 hours

measurement time, very sensitive methods are necessary. Especially methods eliminating uncertainty of temperature monitoring are desirable. Following the ideal gas equation a temperature uncertainty of 0.1 K, which is a typical specification of modern temperature sensors, causes an uncertainty of the pressure determination of 1 mbar. Regarding the leakage rates in table 3.1 this number is in the region of 100% or more. A measurement with reasonable significance can not be given within the required 24 hours. At least a sensitivity of 0.3 mbar or less is desired for a useful method.

3.2 Methods

The aim is an easy-to-use series measurement of the leak rate, both, for single tubes and MDT chambers. For single tubes it requires the test of about hundred tubes a day and for chambers shortly prior installation in UXA about ten units should be checked every day.

Several techniques have been considered to measure/detect gas leaks, e.g.

- Brandeis method,
  (test volume inside a vacuum, of which the pressure is monitored over a time period)
- water bath method,
- gas sniffer,
- manometer,
- mass spectrometer and
- MDT gas leak self test (based on method proposed by [17]).

All these techniques have already been tested. For obvious technical reasons we do not discuss the Brandeis method, the water bath method and the use of a gas sniffer any further. For leak tests too much work, manpower and time is needed to put a whole chamber (few cubic meters) into a vacuum storage or water bath, where the electronics have to be dismantled making impossible the simultaneous read out of the chambers. The last three methods are to use a manometer, a mass spectrometer or the 'MDT gas leak self test', which uses the dependency of the gas gain on the gas density (gas gain method). These remaining methods are only tests on the gas tightness and not usable for gas leak detection. Gas leak localisation is only possible with helium leak sniffer or the water bath method. The method discussed in this thesis is the 'MDT gas gain test' based on the idea of the group at Protvino [17], where the tube is used as a self testing device.

3.2.1 Differential Manometer

The differential manometer consits of two volumes, which are separated by a membrane, which has a mechanical connection to a resistor or capacity. The advantage of differential

manometers over absolute measuring manometers is the reduced sensitivity on temperature. For pressure determinations of 1 mbar or less this argument is not valid any more. For chamber testing a temperature measurement for the very inner tubes is not possible. But referring to the ideal gas equation an uncertainty of 0.1^oC leads to an uncertainty of 1 mbar. For a relative sensitivity of desirable 50% measurements take already a few days using the differential manometer. In temperature controlled space the use of a differential manometer might be sensitive enough.

3.3 The Principle of Operation of the Gas Gain Method

Since MDT chambers are wire chambers, the ionisation caused by primary particles (photons, muons, electrons, ...) is amplified by gas multiplication near the wire and a current signal on the anode wire is induced (Figure 1.13).

The gas gain, the amplification of the primary ionisation, is caused by the applied electric field between anode wire and tube wall. The current signal on the wire caused by a single primary particle, e.g. a muon, is measured with a charge ADC. The total deposited charge on the wire per primary particle is dependend on the properties of the primary particle, of the gas and of the electric field. The obtained total deposited charge is plotted in a pulse height spectrum for a certain number of primary particles ($\approx 10^6$). The change of the gas density inside the tube can be obtained from various pulse height spectra at different gas pressure, where the peak shift of the most probable value is determined. The gas gain gain as a strong function of the density is used. This procedure of measuring the gas tightness of MDTs and MDT chambers using the tubes itself as sensitive devices is called the "Gas Gain Method".

In the following sections the process of primary ionisation and the gas gain is explained in detail. Further, different effects interferring on the gas gain and hence the density measurements are discussed. The limits of the method are shown in Section 3.6.

3.3.1 Energy Loss of Particles in Matter

Energy Deposition by Charged Particles

The most probable energy loss per unit of path length is computed by the summation of the energy lost to all electrons of atoms in the vicinity of the incident particle with charge Z and mass m. It is given by the Bethe-Bloch formula

$$\frac{dE}{dx} = \frac{4\pi N e^4}{mc^2}\frac{1}{\beta^2}z^2\left(ln\frac{\sqrt{2mc^2E_{max}}\beta\gamma}{I} - \frac{\beta^2}{2}\right) , \tag{3.1}$$

where E_{max} is the cut-off energy and I the ionisation potential [18].

Photon Detection

Like for charged particles, the electromagnetic interaction also allows the detection of photons. In this case the interaction is a single localised event. The attenuation of a beam of photons traversing a thickness x of a medium with a density ρ is given by $I = I_0 * e^{\rho\mu x}$, where μ is the photon absorption coefficient that depends on the photon energy and the medium (Section 4.2.1). Depending on the photon energy, the interaction can follow different mechanisms. At low energy, up to several keV, the dominant process is photo-electric conversion; then Compton scattering takes over, up to energies of a few hundred keV, and at even higher energies electron-positron pair production is the most probable process. The pulse height spectrum caused by the two effects at lower energies can be seen in Figure 4.2.

3.3.2 The Gas Gain

The total deposited energy is amplified by the applied E-field in the drift tube. The amplification factor, the gas gain G, described by the Diethorn formula [18],

$$G = \left(\frac{V}{ln\left(\frac{b}{a}\right) a E_{min}(\rho_0) \frac{\rho}{\rho_0}} \right)^{\frac{ln(2)V}{ln\left(\frac{b}{a}\right)\Delta I}} \tag{3.2}$$

is dependent on the gas density ρ inside the tube, where a is the wire radius (a=25μm), b the inner tube radius (b=1.46 cm), V the anode voltage and ΔI the ionisation potential. As the gas mixture is Ar/CO_2 93/7 the Diethorn parameters are $E_{min}(\rho_0)$=24 kV/cm and ΔI=34 V [19]. The MDTs will be operated at a pressure of 3 bar absolute and a high voltage of V=3080 V, corresponding to a gas gain of $2 * 10^4$.

The dependence on the density can be used to determine leak rates of MDT volumes. Changes of the gas gain G can be detected in the pulse height distribution, which is recorded with an charge ADC.

3.3.3 Density-Dependence of the Gas Gain

The gas gain G is a steep function of the density. A density variation $\Delta\rho$ will change the gain by

$$\frac{\Delta G}{G} = -\frac{ln(2)}{ln\left(\frac{b}{a}\right)} \frac{V}{\Delta I} \frac{\Delta\rho}{\rho} \ . \tag{3.3}$$

With above mentioned working points a gas density variation leads to a change in the gas gain of $\frac{\Delta G}{G} \approx -9.85\frac{\Delta \rho}{\rho}$.

The method uses the measurement of the relative peak shift in the spectrum of the pulse height distribution of cosmic muons or photon radiation. The peak position A is determined by a fit resulting in $\frac{\Delta A}{A} = \frac{\Delta G}{G}$, where G is the gas gain of equation 3.2.

3.3.4 Temperature Effects

The temperature influences the gas density inside a tube or chamber in two ways. On the one hand due to a change of the absolute temperature the aluminium tube defining the gas volume changes. Secondly, a temperature gradient over the measured volume causes a density gradient since the pressure equilises. Hence temperature variations causing changes of the temperature gradient will result in local density variations. The local density variations are similar to the difficulties with the usage of the differential manometer, but in the case of the gas gain method can be easily avoided.

Absolute Temperature

The relative thermal expansion coefficient of aluminium is $24 * 10^{-6}/K$. For a cylindrical volume a temperature variation will change the density by

$$\frac{\Delta \rho}{\rho} = -\frac{\Delta V}{V} = -(24 * 10^{-6}\Delta T - 1)^3 = \\ -3 * 24 * 10^{-6}\Delta T \ + ... \approx -7.2 * 10^{-5}\Delta T \tag{3.4}$$

.

With temperature sensors, variations can be determined with an accuracy of $\pm 0.1K$. The uncertainty $\frac{\Delta \rho}{\rho} = -7.2 * 10^{-6}$ by thermal expansion is more than one magnitude below the desired sensitivity of $\frac{\Delta p}{p} = 3.3 * 10^{-5}$.

In figure 3.2 the temperature distribution of the BOL located in DATCHA/BA5 is given. It shows the temperatures along the x-axis of the chamber and the variations versus time (7 days). The scaling of the first axis are sensor indices. As the sensors were not uniformly distributed over the chamber the approximate location is given on top of the figure. The temperature increase near the FE electronics is even steeper than it seems to be. The maximum temperature difference on the chamber is about 3 K. These measurements have been done with BIMUX electronics mounted on the chamber. They radiate a few times more heat than the final electronics will do.

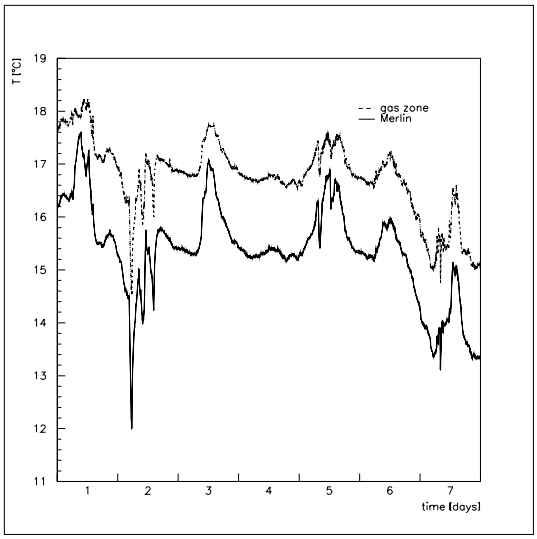

Figure 3.1: Temperature trend in X5

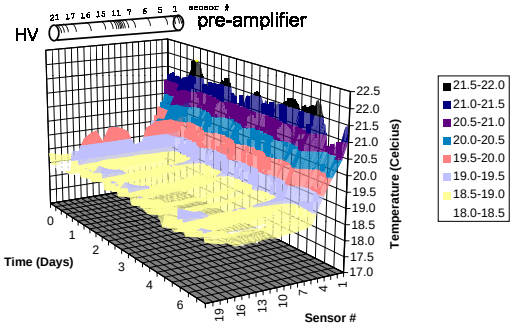

Figure 3.2: Temperature distribution of a BOL chamber

Local Density Variations

The second temperature effect due to variations of the temperature gradient in the common volume is an effect, which occurs, if radiation is not uniformly distributed over the measured volumes. This problem occurs in the case of single tube testing as discussed in chapter 4.2.

Because of the small surface of single tubes and the low density of cosmic muons radioactive sources are needed to achieve the necessary statistics. In the case the source is not evenly distributed over the measured volume, only the local density in the region of the photon beam determines the recorded spectra. Variations of the temperature gradient along the tube change the local density in the region of the photon beam. In the spectra density fluctuations are recorded, which might be wrongly interpreted as a result of gas leaks. Uniform irradiation or a temperature stabilisation have to be used.

A good approximation of the evenly distributed source is a bulk source, which is moved constantly with a certain frequency along the tube. For a rough estimation the temperature distribution (equation can be approximated with an offset (1st term), a time dependency of the offset (2nd term), a linear temperature gradient (3rd term) and its time dependency (4th term).

$$T(x,t) = T_0(x=0) + \Delta T\, t + grad_T x + \Delta grad_T x\, t \tag{3.5}$$

$\Delta T[\frac{K}{h}]$ describes the change with time, $grad_T[\frac{K}{m}]$ and $\Delta grad_T[\frac{K}{mh}]$ represent the linear gradient and its time dependence. The average temperature $T_{average}(t)$, which is directly correlated to the average density, is then defined as

$$T_{average}(t) = \frac{\int_0^l T(x,t)dx}{l} \ , \tag{3.6}$$

where l is the tube length. Assuming a $\Delta T = 0.1\frac{K}{h}$ and $\Delta grad_T * l = 0.1\frac{K}{mh}m$ and a caused error of $\Delta T_{average}(t) = T_{average}(t) - T_{average}(t=0) < 0.01K$, what is equivalent to 0.1 mbar, the maximum allowed crossing time over the tube is 4 minutes.

These assumptions of temperature fluctuations are valid inside an air conditioned room, but not if a heat source (e.g. human being, ...) enters the room and approaches the measured volume.

3.3.5 High Voltage

Like the density, the fluctuations of the high voltage have big influence on the gas gain. Building a tube, which is meant to be used as a reference volume, where the peak change $\frac{\Delta A}{A}$ is only dependent on the HV, the limitation by HV can be eliminated (chapter 3.4).

The gas gain changes with high voltage in the following way:

$$\left(\frac{\Delta G}{G}\right)_V = \frac{ln(2)\left(1 + \left(\frac{V}{ln\left(\frac{b}{a}\right)aE_{min}(\rho_0)\frac{\rho}{\rho_0}}\right)\right)}{ln\left(\frac{b}{a}\right)\Delta I}\sigma_V \ . \tag{3.7}$$

A limit to the sensitivity of the gas gain method is the instability of the HV voltage. Deriving from the Diethorn formula an uncertainty of the gas gain is given by equation 3.7 due to high voltage fluctuations. For Ar/CO_2 93/7 (3 bar) and a HV of 3.1 kV one calculates $\sigma\left(\frac{\Delta G}{G}\right) = 10^{-2}\sigma(V)$. For a sensitivity of the relative pressure drop determination of 0.3 mbar a HV supply with $\sigma\left(\frac{\Delta V}{V}\right) = 0.3 * 10^{-4}$ is needed. Commercial HV supplies achieve a stability of less than 50 mV (at 3600kV) which is even below the required specification. With this specifications for the HV stability the sensitivity is limited to 0.2 mbar. In this study no reference volume was used.

3.4 Reference Volume

The specifications of the reference tube are the following. The dimensions have to be equal to those of the measured tubes, except the length. So this concerns wire radius and inner tube radius. Materials can be chosen as needed as they do not influence the behaviour of energy deposition and gas gain and so the signal in the FE electronics. The reference tube should be 'absolute' tight. In that case fluctuations of the $\frac{\Delta G}{G}$ in the spectra of the reference tube can only be due to HV fluctuations. The materials and the construction has to be chosen to this specification. Gas leakage specification for the reference tube is $\Delta\rho < 10^{-9}\frac{bar\ l}{s}$, at least one magnitude below the specification of the MDTs as written

in [15]. Construction should be different to those used 'normally'. As tube material steel is proposed. The end plugs should be of ceramic and method of 'crimping on the O-ring' is not recommended. The use of such a reference tube would make it possible to improve the sensitivity below 0.2 mbar.

Initial Gas Density

One source of errors could be the difficulty to fill two separate volumes with exactly the same average density. This is obvious, as it is not easily possible to have the two volumes within a temperature gradient of 0.1^oC. Different initial densities in the two volumes lead to different behaviours in $\left(\frac{\Delta G}{G}\right)_V$. So one estimates the maximum density difference which can be allowed in a negligible difference in the gas gain trend. With equation 3.7 one calculates

$$\frac{\rho}{\rho_o} = \frac{ln(584)\ V}{E_{min}\ e^{\frac{39\ \ ln(584)\left(\frac{\Delta G}{G}\right)_V}{ln(2)\ \ \sigma_V} - 1}} \ . \tag{3.8}$$

Assuming that the error $\frac{\Delta G}{G}$ caused by the error of the initial density should be less than 10^{-5}, this occurs in a maximum allowed error of density $\frac{\Delta\rho}{\rho} = 0.33 * 10^{-2}$, which equals a $\Delta p = \pm 10\ mbar$ (temperature corrected) at 3 bar. $\frac{\Delta G}{G}$ was chosen in a way, that the error is one magnitude below the desired accuracy of the whole method. It was also assumed that the long term stability of the HV supply is $\pm 1V$.

These specifications requires, if the two volumes are filled with the same gas supply, so at the same pressure, that the temperature difference does not exceed $\pm 1^oC$.

3.5 Trigger

An external trigger is not needed. It would need to much effort and manpower to install a trigger chamber at every tested chamber and does not provide any advantages. A simple self trigger setup is sufficient. The appearance of an additional peak, the pedestal of noise trigger, does not represent a problem.

A certain pedestal peak is even desired. Variations of the pedestal due to the electronics of the ADC are monitored permanently. A pedestal can be generated artificially by switching the discriminated signal line and a pulse generator. Also the pre-amplifiers do not have variations an absolute stable amplification behaviour due to temperature. This can be monitored by using simultaneously a pulse generator on the test pulse input of the pre-amplifiers.

3.6 Statistical Error of the Spectra

Pulse height distributions either of cosmic muons, which can be described by a Landau distribution (figure 4.1), or of photons from a radioactive source (figure 4.2), which have Gaussian-like shapes, are recorded to determine the peak shift due to density changes. The spectra do have a statistical error, which is dependent on the spectrum shape and the number of entries.

The determination of the leak rate is given by equation 3.3. The error of the peak σ_A evaluated by a fit function results in an uncertainty of the density of

$$\sigma_{\frac{\Delta\rho}{\rho}} = \frac{ln\left(\frac{b}{a}\right)}{ln2}\frac{\Delta I}{V}\sigma_{\frac{\Delta A}{A}} \approx \frac{1}{10}\sigma_{\frac{\Delta A}{A}} \ . \tag{3.9}$$

For small peak shifts the approximation $A_f \approx A_i = A$[1] is valid and the resulting error calculates to

$$\sigma_{\frac{\Delta A}{A}} = \sqrt{\left(\frac{1}{A_i}\sigma_{A_f}\right)^2 + \left(\frac{A_f}{A_i^2}\sigma_{A_i}\right)^2} \approx \frac{\sqrt{2}}{A}\sigma_A \ . \tag{3.10}$$

The error of the peak σ_A can be estimated using the FWHM σ_{Gauss} and the number N of entries for the Gaussian fit. For a Landau distribution an equivalent FWHM can be estimated by $\sigma_{Landau} = \frac{A}{2}$, where A is again the peak position. This approximation leads to a required number

$$N = \left(\frac{ln\,584}{ln\,2}\frac{\Delta V}{V}\frac{\sqrt{2}}{A}\frac{\sigma_{Gauss}}{\sigma_{\frac{\Delta\rho}{\rho}}}\right)^2 \tag{3.11}$$

of entries in the pulse height distributions for a certain sensitivity $\sigma\left(\frac{\Delta\rho}{\rho}\right)$. For an accuracy of the relative density drop $\frac{\Delta\rho}{\rho} \approx 10^{-4}$ using the 17 keV peak of the ^{241}Americium with molybdenum the number of entries has to be about $0.5 * 10^6$. About the same number is necessary in the cosmic muon spectrum.

3.6.1 Limits on Sensitivity of Leakage Tests

The required measurement period of a group of tubes should be T hours. The tubes are read out permanently. The source deposits x hits per hour on one tube. So the number r of spectra with N entries is

[1] i ... initial, f ... final

$$r = \frac{x}{N}T \ . \tag{3.12}$$

For a run of two spectra (initial i and final f spectrum) the accuracy of the relative peak shift $\frac{\Delta G}{G}$ is given by equation 3.6. For a continuous recording of spectra there are r/2 pairs, which represent the relative density drop in a time interval T/2. By Gaussian evaluation of the r/2 measurements one estimates for the sensitivity of the relative density drop

$$\sigma_{\frac{\Delta\rho}{\rho}} = \frac{ln\left(\frac{b}{a}\right)}{ln2}\frac{\Delta I}{V}2\frac{\sigma_{\frac{\Delta A}{A}}}{\sqrt{\frac{r}{2}}} \ . \tag{3.13}$$

With the assumption $\sigma_{\frac{\Delta A}{A}} \approx \frac{\sigma_{Spectrum}}{\sqrt{N_{fit}}}$ the sensitivity becomes independent on number of entries in the fit. Only the hit rate x and therefore the activity of the radiation source is essential.

$$\sigma_{\frac{\Delta\rho}{\rho}} \approx \frac{4}{10}\frac{\sigma_{Spectrum}}{A}\frac{1}{\sqrt{xT}}\frac{N}{N_{fit}} \tag{3.14}$$

For a source like in X5 as specified in 4.2.1 the number of photons is $10^6\frac{hits}{h\ tube}$. Only 30% of the entries are in the peak of 17 keV photons (50% in the 60 keV peak and 20% of Compton electrons). For cosmic muons the error in the peak $\sigma_{\frac{\Delta A}{A}} = \frac{\sigma_{Spectrum}}{A} \approx \frac{1}{2A}$ is about twice as much as for 17 keV peak of the photons from the molybdenum. The hit rate for one multilayer of a BIS is about $10^7\frac{hits}{h}$. By this the sensitivity in both cases of 17 keV photons and cosmic muons is $\sigma\frac{\Delta\rho}{\rho} < 10^{-4}\frac{1}{\sqrt{T}}$. The commonl estimation is possible due to the different hit rates and different ratios $\frac{\sigma_A}{A}$, which result in the same sensitivity. In full accordance to the setups proposed in Chapter 4 and the measurements in Chapter 5 one achieves a sensitivity of $\frac{\Delta\rho}{\rho} = 0.5 * 10^{-4}$. This translates to $\sigma\left(\Delta\rho\right) \approx 0,2mbar$. According to Table 3.1 the sensitivity of the leak rate measurment is below $0.5{*}10^{-8}\frac{bar\ l}{s}$ even for measurement times of only T = 16 hours.

In calculation of the error propagation the effects of HV fluctuations and uncertainties of the temperature have not been included for the following reasons. The HV fluctuations have never been observed in the experiment. This might have the following reason: The HV fluctuations are of a high frequency and are not big enough to influence the determined peak position. The effect causes only a negligible broadening of the peak. The temperatures effects are one magnitude below the required sensitivity of the gas leak rate, if the room temperature is monitored with an accuracy of $\pm 0.1\,K$.

Chapter 4

Series Test of MDTs and Chambers

4.1 Chamber Leak Testing

The proposed scenario is the following: MDT chambers are delivered to CERN and stored. Shortly before being installed in the ATLAS experiment they are checked again for functionality and quality. Chambers are already equipped with FE electronics and filled at a gas pressure of 3 bar. With connecting off-chamber electronics and HV supply a leak test with the gas gain method can be performed, in addition to other control procedure like tube testing, HV tests, etc. About 10 MDT chambers per day are to be installed in ATLAS and the same number has to be tested. So, a fast and manpower-economic procedure is needed.

The gas gain method is only capable to detect the average leakrate of one multilayer, because each multilayer has its own input and output valves and all the tubes of one multilayer are connected, .

4.1.1 Cosmic Muons

The spectrum of cosmic muons in Figure 4.1 was recorded using a prototype chamber ('Merlin', see Section 5.1). It shows a characteristic Landau spectrum. Besides this, on the left hand side is a Gaussian peak, which is due to the self triggering setup at the X5, where Merlin was operated. This peak represents the pedestal. On the right side in the last bin are all entries of overflow collected. Both do not disturb the measurements in any way and can be tolerated. The peak of the muon spectrum is at 19 keV and as mentioned in Section 3.6 the FWHM is estimated as $\sigma \approx$10 keV.

The fitted function is an approximation of the Landau distribution. The number of entries in the bin of energy E with the bin width of dE is

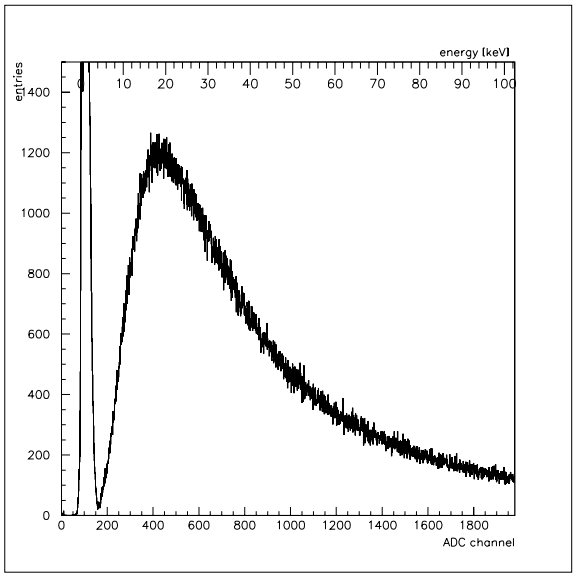

Figure 4.1: pulse height spectrum of cosmic muons

$$\frac{dN(E)}{dE} = a * e^{-d\left[b(E-c)+e^{-b(E-c)}\right]} \tag{4.1}$$

The most probable energy value of this function is expressed by the parameter c ($\approx 19keV$). The parameters a, b and d depend on the bin width and the total numbers of entries of the pulse height spectrum. With $A_{Landau} \approx 2\sigma_{Landau} \approx 2\sigma_{Gauss}$ the error on the peak parameter can be estimated by $\sigma_{peak} \approx \frac{\sigma_{Gauss}}{\sqrt{N}}$, where N is the number of entries used for the fit.

The use of cosmic muons as a radiation source for chamber tests is appropriate for two reasons: On one hand the irradiation of the chamber by a bulk source raises the problem of the local density variation (Section 3.3.4). The average of the density in the whole chamber is recorded in the pulse height spectrum, because the cosmic muons are equally distributed over the surface. On the other hand the rate of cosmic muons is sufficient for the needed sensitivity (Section 3.6). Variations of the cosmic muon spectrum over day and night are of course given, but as the change of the relative intensity dN/dE is important and not the rate dN/dt, this effect has no influence.

4.1.2 Layout

For chamber testing no special hardware is needed. A MDT chamber is completely equipped for the proposed method of testing. The chamber will be equipped with all components before being put into the UXA. The number of off-chamber read out electronics is determined by the number of chambers tested per day. This concerns especially high voltage supply and the electronic crates for the readout.

4.2 Single Tube Testing

Single tube testing has to be performed at the production sites before chamber assembly. About a hundred tubes should be tested a day and testified according to the accepted quality control specifications. For single tube testing two issues are of special interest. As the surface of a single tube is very small and the rate of cosmic muons is not sufficient for proper statistics, radioactive sources have to be used. The arrangement of tubes has to be chosen in a way that the radiation of the source and the molybdenum foil causes the desired peak in the pulse height spectrum.

Section 4.2.1 deals with the layout of the source in greater detail. In Section 3.3.4 a problem caused by using a bulk radioactive source, which irradiates only part of the tube, was discussed. In chapter 4.2.2 a proposal for a tube setup shown.

4.2.1 Radiation Source

A radioactive source very suitable for this method is ^{241}Americium. It is used in combination with a molybdenum foil. For ^{241}Americium the half life time is 432 years and it has only one main peak at 60 keV (35 %, gamma). The second peak at 17 keV with a better $\frac{\sigma}{A}$ ratio is caused by placing a molybdenum foil between source and tube. ^{241}Americium is highly toxic and only available as a closed bulk source.

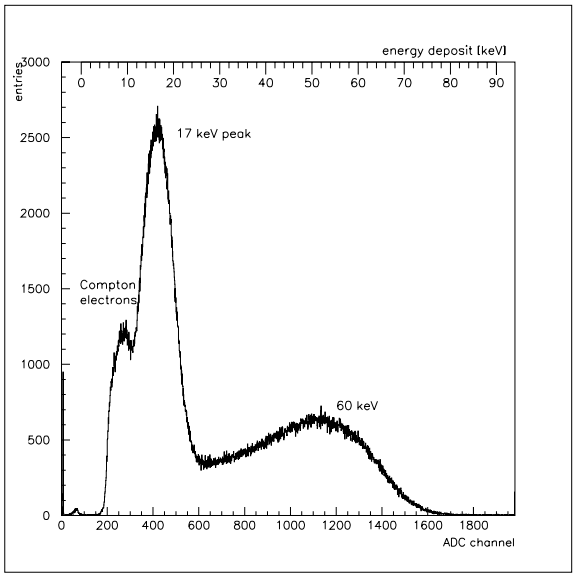

Figure 4.2: Pulse height spectrum of ^{241}Americium with molybdenum foil(0.005 mm)

The lowest energy peak in the ^{241}Americium spectrum comes from the Compton effect, which absorption coefficient is about five times smaller than the one of the photo-effect for 60 keV photons. The upper limit of the energy of the Compton electrons is at 11 keV.

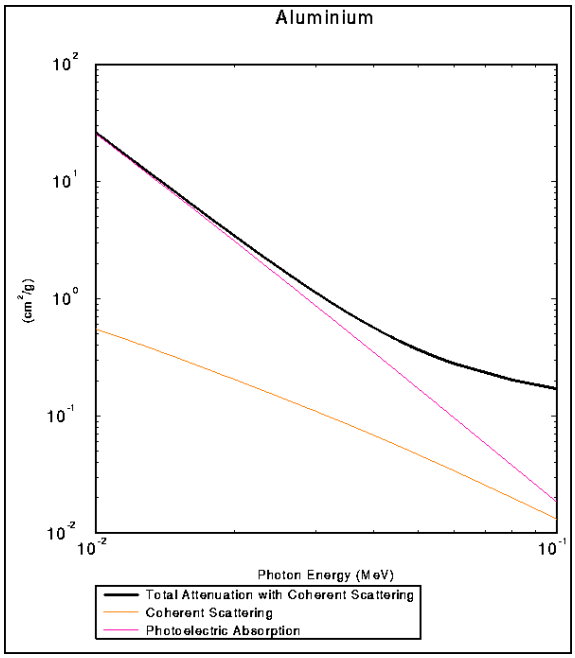

Figure 4.3: photon cross section for Aluminium

$E_{primary\ \gamma}$	17 keV	60 keV	$\rho\ [\frac{g}{cm^3}]$
Mo	$1.83 * 10^1$	$3.97 * 10^0$	10.28
Al	$5.12 * 10^0$	$7.11 * 10^{-2}$	2.7
Air	$7.42 * 10^{-1}$	$8.7 * 10^{-3}$	$1.2 * 10^{-3}$
Ar/CO_2	$1.19 * 10^1$	$2.61 * 10^{-1}$	$1.784 * 10^{-3}$

Table 4.1: photon absorption coefficients in $[cm^2/g]$

Source Layout

In order to determine the dimensions of the source needed to achieve the afforded sensitivity it is necessary to estimate the absorption in the different mediums traversed by the 17 keV and 60 keV photons.

A commercial ^{241}Americium bulk source with a certain activity emits about 20% less photons in 4 Pi than the actual activity. For a 37 MBq source this gives $2.5 * 10^6 \frac{photons}{s\ steradian}$. The percentage of photons in direction of the target, the tube, can be easily calculated.

Material	absorption length [cm]	$\frac{I}{I_0}$ (17 keV)	$\frac{I}{I_0}$ (60 keV)
Mo	0.005	0.39	0.82
Al	$0.04*\sqrt{3}$	0.38	0.986
Air	15	0.986	0.999
Ar/CO_2 (3 bar)	2.5	0.85	0.997

Table 4.2: relative absorption for photons of the indicated primary energy

The absorption of 60 keV photons in air, Ar/CO_2 and Aluminium is negligible. Passing through 0.05 mm of molybdenum the intensity decreases by about 20%. This effect causes the desired 17 keV peak in the pulse height spectrum. The emission of photons is equally distributed in 4 Pi. Increasing the thickness of the molybdenum foil above 0.1 mm does not change the ratio between the 60 keV and the 17 keV part of the spectrum, because the probability of 17 keV photons passing through molybdenum is already very low for this absorption length. Also the intensity of 60 keV photons after passing three foils should still be high enough to achieve proper statistics. It has to assured that in the direction of 60 keV photons from the source to the tube in the whole sphere a molybdenum foil has to be placed. In other cases the rate of 17 keV photons is relatively too small over 60 keV photons and the 17 keV peak can not be determined any more.

In Figure 4.4 a schematic view of the photon absorption is given for a minimum setup, which can be easily extended for more complex arrangements of several tubes. A ^{241}Americium source emits mainly gammas of 60 keV, which descend from an α-decay.

Table 4.1 and 4.2 show the absorption coefficients for the two photon energies and the intensity loss for typical absorption lengths trough the various mediums. Hence the count rate of the tubes can be estimated roughly. A source with an activity of 37 MBq is sufficient for the setup proposed in Section 4.2.2.

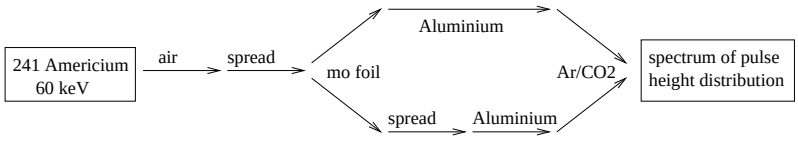

Figure 4.4: photon decay of a minimum setup

4.2.2 Single Test Layout

Several ideas were considered for an arrangement to expose an adequate number of tubes to the irradiation of the source. Two requirements have to be taken into account. There should be the use of a minimum number of sources due to costs. Secondly, the absorption peak of the molybdenum source has to be as much distinctive as possible from the remaining spectrum to obtain the best possible fit. The absorption of the two main photons of 17 and 60 keV through the different mediums are given in Table 4.1.

An arrangement of the tubes in a horizontal angle covering 360^o is not possible. The ^{241}Americium is highly toxic and no supplier provides a bulk source radiating a sphere of 4*Pi. The maximum radiation angel is a hemisphere. Also the position(s) of molybdenum foil has to be mentioned. Since the absorption length of aluminium for 17 keV photons is very small, only about 40% of the emitted 17 keV photons traverses the tube wall. Consequently in a second layer of tubes the 60 keV photons dominate. The peak of 17 keV photons almost disappears and no information can be obtained any more. By placing several foils between the tube layers one can keep the ratio of 17 keV and 60 keV photons almost constant for all tubes. The absorption of 60 keV photons by the molybdenum foil leads to an ensity decrease by about 20% in each layer. The photon emission by the molybdenum

foil is flat distributed over the total sphere, also the tube already penetrated by 60 keV photons is irradiated by the 17 keV photons from the foil 'behind' it. This makes it possible to reduce the number of foils and to increase the number of sufficiently irradiated tubes by a factor of two(Figure 4.5).

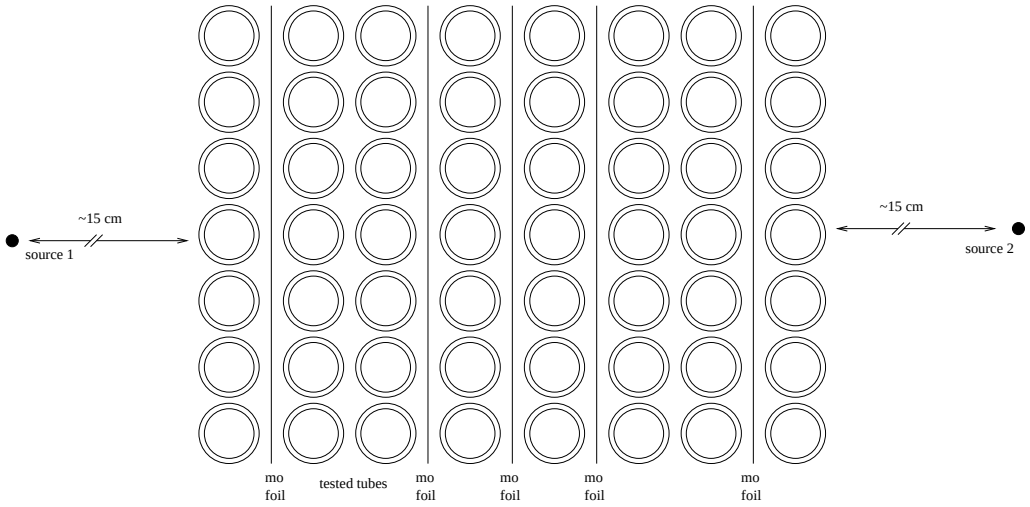

Figure 4.5: schematic view of tube setup

As already mentioned the ratio of 17 and 60 keV photons is essential for the accuracy of the spectrum fits. The maximum accuracy is achieved if the irradiated area on a tube is completely covered by a molybdenum foil. It does not matter if the foil is placed before or behind the tube looking in beam direction. Increasing the thickness of the molybdenum foil only decreases the hit rate of photons in the tube.

The problem of local density variations (Section 3.3.4) can be handled in several ways. Moving the source with a certain frequency along the tube or placing several bulks along the wire axis results in an almost uniform irradiation. This solutions are not desirable because of the mechanic effort in the first and the number of bulk sources in the second case. A convenient way is to place the tested tubes into a box, e.g. made of styro foam. This reduces the temperature gradient to the required level.

4.2.3 Gas System

The handling of the setup is an important issue as the number of tubes is very large and should not be labor intensive. A permanent gas distribution and supply is not needed. The test itself runs at closed tube inputs. The arrangement of the tubes is very compact and so the use of conventional ball valves takes a lot of space, makes the mounting of HV and R/O cards impractical and inefficient. In Figure 4.6 a drawing of a tool is shown, which is adapted to the needs for single tube tests. The handling of the tubes becomes very easy.

The bronze tool is an all-in-one component. It serves as a self closing device after the tube is pumped to the pressure of 3 bar and as a connection between the anode pin and the HV card. The connection of the ground pin is still possible. The tool is used only on one side of the tubes.

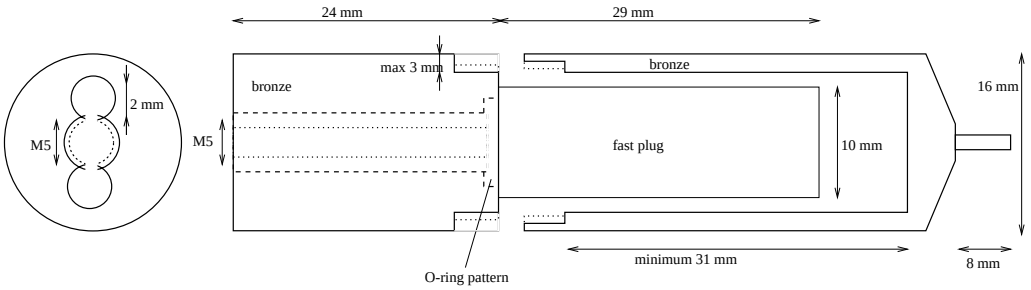

Figure 4.6: schematic view of the bronze connector

The procedure of filling the tubes with Ar/CO_2 is the following: The left part of the bronze tool is fixed on one side of the tube. After flushing the tube at the far end of the tool the tube is closed in the way as designed for ATLAS MDTs. One uses a bronze ring instead of the normally used connector to the gas manifold and the signal cap. If the pressure raised then to 3 bar the gas supply is disconnected from the bronze tool. The part is equipped with a fast plug[1] (Figure 4.6). The fast plug closes its built-in ball valve at the time of disconnection from the gas supply. Fixing the second part of the bronze tool makes it possible to use the HV cards designed for ATLAS. The tube is now a stand-alone device regarding the gas system.

[1]SERTO, CO KA 203-M5 N, provided by GRESSEL AG (CH), http://www.serto.com

Chapter 5

Performance Test on MDTs and Chambers

For a validation of the proposed methods two setups were built next to X5 of the west experimental hall. A MDT chamber called Merlin, which was previously built to perform ageing tests, has been reactivated for leak tests on MDT chambers. In the control room itself a configuration of two MDTs served as a proof for the single tube method.

5.1 MERLIN

Merlin is a MDT prototype chamber, which is placed next to X5 in the west area hall. It was built to perform ageing tests. The chamber does not have a typical shape of one of the barrel chambers, but is very similar. It consists of 96 MDTs (length 3.8 m), which are assembled in groups of 24 tubes (Figure 5.1). Each group can be connected to the gas system by individual valves. One quarter of the tubes is not usable, because the end plugs in this section (L2) show enormous cracks. The remaining tubes together with its on chamber gas system show a reasonable leak rate to perform gas tests on it. The leakrate of Merlin was determined to be 2.2 mbar/h. The uncertainty on this value is negligible, as the test was performed with a digital manometer ($\pm 1\,mbar$) and for a period of several days. The initial parameters of the gas were Ar/CO_2 90/10 at a pressure of 3 bar absolute.

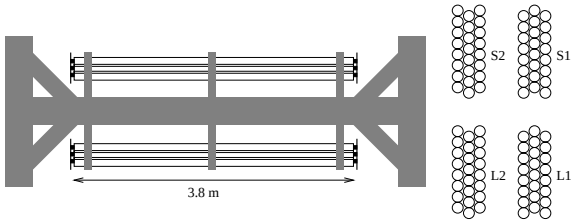

Figure 5.1: MERLIN: Top view and vertical cut through the arrangement of MDTs

The on-chamber electronics consist of BNL amplifiers on the R/O side and HV cards. The remaining R/O chain consists of shaper, analog and digital NIM electronics, an ADC and a

CPU on a VME crate. Each signal was split 3 times in an analog way. One readout channel went directly into one of the 12 ADC channels (LeCroy 2249W, 11 bit, maximum count 1980 channels (-512 pC)). Another channel goes through the discriminator (threshold 60 mV) and a coincidence unit (gate 800 ns) and generates the gate signal for the ADC. Because of this self trigger a peak at the pedestal is generated (Figure 4.1). The ADC is read out by the VME CPU and the data acquisition software was BIRDIE [20].

As drift gas mixture of Ar/CO_2 90/10 at a pressure of 3 bar absolute was used. The tube was operated at a high voltage of 3100 kV, the test was performed with cosmic muons.

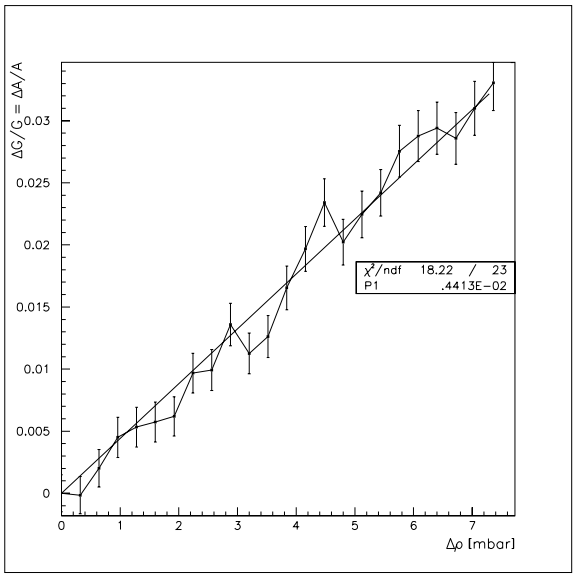

Figure 5.2: relative peak shift versus density drop

5.2 Single Tube Test in X5

The aim of this second experiment was not only to apply the gas gain method on single tubes, but especially to check the design and handling of the bronze tool with its fast plug.

The tested object was a MDT tube of the type BOS (length 4990 mm), wired and crimped by the prototype wiring machine at CERN. The design of the end plugs is as given in CDD ATLMMACA0025 and 27. For this end plugs the fast plug device was built as described in section 4.2.2. This tool was mounted on the HV side. The connection of the R/O cards is the same as foreseen for ATLAS, using the signal cap. Instead of a connection to a gas manifold a blind bronze ring is used to close the tube. The filling procedures takes about 15 minutes. Gas flow goes in on the HV side and flushes the whole volume for about ten minutes. The R/O side is closed with the blind ring and the signal cap while low gas flow. After another five minutes the pressure inside the tube stabilises at 3 bar and the gas supply is disconnected by the fast plug. Mounting on-tube cards finalises the procedure and R/O begins. BNL single channel cards as for ageing tests were used. The DAQ is the same as for the chamber leak test described in Section 5.1.

Pulse height spectra were recorded as shown in Figure 4.2. The peak shift determined by Gaussian fits is plotted in Figure 5.3. The shown error bars are the ones obtained from the fit itself. They are of the size as estimated in Section 3.6. For this run with a hit rate of $10^6 \frac{hits}{h\ tube}$ and within 10 hours a sensitivity of the leak rate of 0.3 mbar was achieved.

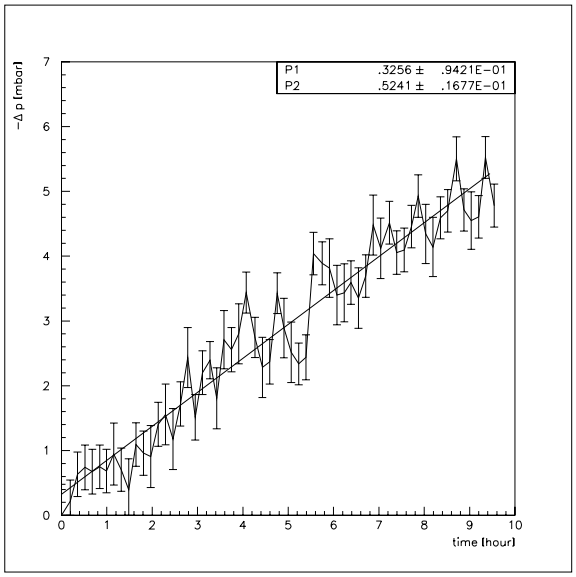

Figure 5.3: pressure drop of a MDT

In Figure 5.3 a representative measurement is shown. The hit rate of photons emitted by ^{241}Americium were slightly higher than supposed in a setup designed for a group of about 60 tubes. The source was located next to the sensitive tube. The number of entries in a single spectrum were 10^6. The record of one spectrum took about ten minutes. The single point accuracy is in average 0.8 mbar. Due to the high number of entries within ten hours already at this point the leak rate can be determined as 0.52±0.017 mbar/hour. This is slightly above the required sensitivity of $0.5 * 10^{-8} \frac{bar\,l}{s}$ due to the short time of measurement.

Chapter 6

Conclusion

The quality control of MDTs and chambers should guarantee drift tube devices of highest standards. This is necessary to achieve the ambitious goal of a momentum resolution of $\sim$ 10% for muons with a traverse momentum of p_T=1TeV/c. Quality control includes HV behaviour, tube performance, mechanical properties and gas tightness. A method on gas tightness is topic of this thesis. Besides the mass spectrometer and the differential manometer also the gas gain method is a viable and elegant solution to measure the leak rate of drift tubes.

The determination of the gas tightness of MDTs and MDT chambers can be performed by using the drift tubes as sensitive devices. As the gas gain is strongly dependent on the density the evaluation of pulse height spectra makes it possible to determine the leak rate.

The main advantages of this method are:

- applicable for single MDTs and MDT chambers
- density (and gas gain G(ρ)) are independent on the temperature
- procedure permits integrated test of HV, tube performance and leak tightness
- sensitivity $< 0.5 * 10^{-8} \frac{bar\ l}{s}$ in 24 hours
- needed manpower and costs low

Near X5 in the west area hall of CERN two experiments have been carried out. A prototype of a MDT chamber and single MDTs have been measured on their gas tightness with the proposed method. The designed sensitivity has been achieved for both setups.

Bibliography

[1] G. Jarlskog and D. Rein (editors): *Proceedings of the Large Hadron Collider Workshop*, CERN/90-10 (1990).

[2] DELPHI Collaboration: *Search for Neutral Higgs Bosons in* e^+e^- *Collisions at* $\sqrt{s} =$ 188.7 GeV, submitted to HEP'99 Conference, Tampere (July 1999).

[3] CMS Collaboration: *CMS Technical Proposal*, CERN/LHCC 94-43 (1994).

[4] ALICE Collaboration: *ALICE Technical Proposal*, CERN/LHCC 95-71 (1995).

[5] LHCb Collaboration: *LHCb Technical Proposal*, CERN/LHCC 98-4 (1998).

[6] ATLAS Collaboration: *ATLAS Technical Proposal*, CERN/LHCC 94-38 (1994).

[7] ATLAS Inner Detector Collaboration: *ATLAS Inner Detector Technical Design Report*, CERN/LHCC 97-16 and 97-17 (1997).

[8] ATLAS Calorimeter Collaboration: *ATLAS Calorimeter Technical Design Reports*, CERN/LHCC 96-40, 96-41, 96-42 (1996).

[9] N.P. Hessey: *The precision drift chambers for the ATLAS Muon Spectrometer*, Nucl. Intrum. Methods **A419** (1998) 326-330

[10] G. Viehhauser: *Detector Physics of the ATLAS precision muon chambers*, PhD thesis, CERN (1996).

[11] P. Creti et al.: *Test-beam results from the Calypso MDT chamber*, ATLAS MUON-NO-97-196, CERN (1997).

[12] W. Riegler: *Limits to Drift Chamber Resolution*, PhD Thesis, CERN (1997).

[13] E. Gschwendtner et al.: *Analysis of the X-tomograph scan data for MDT chamber prototypes*, ATLAS MUON-NO-175, CERN (1997).

[14] H. Rieder, A X-ray Tomograph to Measure Mechanical Structures at a 1 Micron Level', Diploma Thesis, CERN 1999

[15] Atlas Muon Collaboration,
ATLAS Muon Spectrometer TDR, CERN/LHCC/97-22

[16] http://atlasinfo.cern.ch/Atlas/GROUPS/
/MUON/mdt/mdt-summary-specifications.pdf

[17] A. Borisov et al., Leak Test of Drift Tube by Means of the Tube Itself, ATL-COM-MUON-99-006, IHEP, Russia, 1999

[18] W. Blum, L.Rolandi, Particle Detection with Drift Chambers, Springer, 1993

[19] M. Aleksa, W.Riegler, Non-Linear MDT Drift Gases like Ar/CO_2, ATL-MUON-98-268, CERN, 1998

[20] N.P. Hessey, http://atlasinfo.cern.ch/Atlas/GROUPS/
/MUON/datcha/datchadaq.ps, 1996